

ASL-TR-0016

AD

Reports Control Symbol  
OSD - 1366

# EFFECTS OF PARTICULATE COMPLEX REFRACTIVE INDEX AND PARTICLE SIZE DISTRIBUTION VARIATIONS ON ATMOSPHERIC EXTINCTION AND ABSORPTION FOR VISIBLE THROUGH MIDDLE-INFRARED WAVELENGTHS

SEPTEMBER 1978

By

**S.G. JENNINGS**

**R.G. PINNICK**

Approved for public release; distribution unlimited



US Army Electronics Research and Development Command

**Atmospheric Sciences Laboratory**

White Sands Missile Range, NM 88002

## **NOTICES**

### **Disclaimers**

**The findings in this report are not to be construed as an official Department of the Army position, unless so designated by other authorized documents.**

**The citation of trade names and names of manufacturers in this report is not to be construed as official Government indorsement or approval of commercial products or services referenced herein.**

### **Disposition**

**Destroy this report when it is no longer needed. Do not return it to the originator.**

REPORT DOCUMENTATION PAGE		READ INSTRUCTIONS BEFORE COMPLETING FORM
1. REPORT NUMBER ASL-TR-0016	2. GOVT ACCESSION NO.	3. RECIPIENT'S CATALOG NUMBER
4. TITLE (and Subtitle) EFFECTS OF PARTICULATE COMPLEX REFRACTIVE INDEX AND PARTICLE SIZE DISTRIBUTION VARIATIONS ON ATMOSPHERIC EXTINCTION AND ABSORPTION FOR VISIBLE THROUGH MIDDLE-INFRARED WAVELENGTHS		5. TYPE OF REPORT & PERIOD COVERED R&D Technical Report
		6. PERFORMING ORG. REPORT NUMBER
7. AUTHOR(s) S. G. Jennings R. G. Pinnick		8. CONTRACT OR GRANT NUMBER(s)
9. PERFORMING ORGANIZATION NAME AND ADDRESS Atmospheric Sciences Laboratory White Sands Missile Range, New Mexico 88002		10. PROGRAM ELEMENT, PROJECT, TASK AREA & WORK UNIT NUMBERS DA TASK NO. 1L161102B53A(SA-3)
11. CONTROLLING OFFICE NAME AND ADDRESS US Army Electronics Research and Development Command Adelphi, MD 20783		12. REPORT DATE September 1978
		13. NUMBER OF PAGES 49
14. MONITORING AGENCY NAME & ADDRESS (if different from Controlling Office)		15. SECURITY CLASS. (of this report)  UNCLASSIFIED
		15a. DECLASSIFICATION/DOWNGRADING SCHEDULE
16. DISTRIBUTION STATEMENT (of this Report)  Approved for public release; distribution unlimited.		
17. DISTRIBUTION STATEMENT (of the abstract entered in Block 20, if different from Report)		
18. SUPPLEMENTARY NOTES		
19. KEY WORDS (Continue on reverse side if necessary and identify by block number) Complex refractive index      Real index of refraction Extinction coefficient      Imaginary index of refraction Absorption coefficient      Middle IR propagation Particle size distribution      Visible and near IR propagation		
20. ABSTRACT (Continue on reverse side if necessary and identify by block number) A comprehensive sensitivity study has been made, using Mie theory, to determine the effect of realistic variations in values of real and imaginary parts of the complex index of refraction on volume extinction and absorption coefficients for a wide range of lognormal particle size distributions (defined by geometric mean radius $r_g$ and geometric standard deviation $\sigma_g$ ). Wavelengths $\lambda$ from visible (0.55 $\mu$ m) through middle-infrared (10.6 $\mu$ m) were considered. Extinction is independent of complex index to within 20 percent for the majority of realistic		

## 20. ABSTRACT (cont)

particle size distributions, providing  $\lambda \lesssim 2\mu\text{m}$ . However, changes in extinction by up to an order of magnitude are caused by realistic variations in refractive indexes for  $2\mu\text{m} \leq \lambda \leq 10.6\mu\text{m}$ , with real index being more important in affecting extinction than imaginary index. Similar changes are caused by variations in particle size distribution for values of refractive indexes typical of atmospheric constituents. For bimodal size distributions representative of desert aerosols, values of the complex refractive index which result in minimum and maximum extinction and absorption coefficients are given. Uncertainty in values of the real and imaginary index of refraction causes less than 20 percent change in extinction for a typical light and heavy aerosol bimodal distribution at visible and near infrared ( $\lesssim 2\mu\text{m}$ ) wavelengths, but causes variation in extinction by up to a factor of about 10 and 3, respectively, for a typical light and heavy bimodal aerosol loading at middle-infrared (9.3 $\mu\text{m}$  to 10.6 $\mu\text{m}$ ) wavelengths. Absorption is generally less dependent on size distribution than is extinction and is more sensitive to complex refractive index than extinction. Absorption is not in general linear with imaginary index, especially for broad particle distributions, and, in general, absorption does not uniquely determine the imaginary index of refraction.

## PREFACE

The results of calculations in this report in tabulated and graphical form constitute an important base of a sensitivity analysis intended to determine how atmospheric aerosols, over a wide range of size parameters and complex refractive index values, limit the battlefield effectiveness of military electro-optical surveillance, target designators, and communications systems.

The authors acknowledge Dr. Marvin Querry, Department of Physics, University of Missouri-Kansas City, and Dr. Dudley Williams, Department of Physics, Kansas State University, Kansas, who supplied raw data on complex refractive indexes of atmospheric constituents. We also acknowledge the help of Dr. H. J. Auvermann in reducing some of the data to graphical form. We gratefully acknowledge Richard D. H. Low and Charles W. Bruce for carefully reviewing this report.

## CONTENTS

	<u>Page</u>
PREFACE	1
INTRODUCTION	3
CALCULATIONAL PROCEDURE	4
EXTINCTION COEFFICIENT AS A FUNCTION OF REAL AND IMAGINARY INDEX OF REFRACTION	5
ABSORPTION COEFFICIENT AS A FUNCTION OF THE IMAGINARY AND REAL INDEX OF REFRACTION	7
Isoabsorption Analysis	9
Extinction and Absorption as a Function of Particle Size Distribution	10
The Spectral Dependence of Extinction and Absorption	11
CONCLUSIONS	13
FIGURES	14
TABLES	25
REFERENCES	38

## INTRODUCTION

Interest in the effect of aerosols on radiative transfer in the atmosphere has grown considerably in recent years. Aerosols affect earth climate, the operation of military electro-optical systems, and high energy lasers. With few exceptions, aerosols are modeled as polydispersions of spheres of uniform composition. In fact, there is considerable compositional variation of aerosol particles depending on local sources and sinks, meteorological conditions, and geographical locale. An aerosol size distribution may consist of several superimposed modes, each mode characterized by different refractive indexes and ranges of particle sizes and shapes. An obvious way to assess the seriousness of approximating a multicomponent aerosol by a single mode is to perform a sensitivity study to investigate the effects of aerosol size and refractive index variations (within a range of values that might be characteristic of different modes) on scattering parameters. This is in part the purpose of this report. A related and perhaps more important reason for a sensitivity study is that definitive measurements of aerosol refractive indexes in the middle-infrared spectral region and aerosol size distributions are not easy to make and consequently are rather sparse. This study reveals what effect errors in measurement and uncertainties in values of aerosol refractive indexes and size distributions have on predictions of aerosol extinction and absorption.

The radiative effects of atmospheric dust in semiarid regions is an example of a research area to which this study applies. Desert aerosols over the Southwestern United States have been shown to be multicomponent [1-4]. Mineralogical analyses of the particles are not always available, and even when they are, knowledge of particle composition does not necessarily imply knowledge of index of refraction. For example, the complex index of the great majority of clay minerals which form a considerable fraction by mass of desert aerosols is unknown in the 3- to 12-micrometer wavelength regime and beyond. Recent measurements by Toon et al. [5] on montmorillonite -- one of the clay mineral family -- indicates that there is considerable variation in both the real and imaginary components of the refractive index from 5 micrometers through the middle-infrared. Similar variations can be expected for the rest of the clay mineral family. Our ignorance of infrared optical constants of desert dust applies to some aerosols of anthropogenic origin as well. In addition, uncertainty as to the validity of past measurements has been emphasized [6].

Similar comments apply to measurements of aerosol size distributions. Measurements for sufficiently broad ranges of particle sizes are few, as are measurements of specific atmospheric constituents, with some exceptions [7-11].

Thus, because of the experimental difficulties associated with measurement of both particle refractive indexes and size distributions, and with the consequential lack of data, investigation of the effect of these parameters on aerosol extinction and absorption is a worthwhile exercise. Such a study for aerosol extinction has been done previously by Bergstrom [12] for a relatively narrow range of refractive indexes and particle sizes.

Atmospheric aerosol size distributions possess geometric standard deviations in excess of 1.25, the upper limit used in the above work. The effect of variations of refractive index on aerosol extinction coefficient has been examined by Hänel and Bullrich [13] using power law distributions. However, their calculations were limited to an upper wavelength value of 2 micrometers. A similar study by Willeke and Brockmann [14] using lognormal model size distributions is useful only for visible or near-visible wavelengths. Atmospheric extinction between 0.55 and 10.6 micrometers due to soil-derived aerosols has recently been calculated by Patterson [15], but the effect of variations of complex refractive index on the extinction was not examined. In this work the authors have chosen a lognormal size distribution representation for a wide range of realistic parameters: namely, geometric mean radii  $0.01 \leq r_g \leq 10 \mu\text{m}$ , and geometric standard deviation  $1.5 \leq \sigma_g \leq 2.5$ . Refractive index values were chosen at 0.55, 1.06, 3.8, and 10.6 micrometers wavelengths to more than adequately cover the range of values of known atmospheric constituents.

#### CALCULATIONAL PROCEDURE

A modified version of the Mie program of Dave [16] was used for scattering calculations in this study, under the assumption that all particles are homogeneous spheres. The Mie theoretical formalisms have been described in well-known works [17-19] and will not be discussed here. The volume extinction coefficient  $\sigma_e$  is calculated according to:

$$\sigma_e = \int_0^{\infty} \pi r^2 Q_{\text{ext}}(x, m) \frac{dN}{dr} dr \quad (1)$$

$N$  is the number of particles with radius greater than  $r$ ;  $Q_{\text{ext}}(x, m)$  is the efficiency factor for extinction and is a function of the particle complex index of refraction,  $m$ , and the size parameter  $x = 2\pi r/\lambda$ , the ratio of the particle circumference to the wavelength. The corresponding absorption coefficient is calculated by replacing the efficiency factor for extinction with that for absorption.

A lognormal was chosen to represent the particle size distribution for several reasons. It has been shown to represent both desert [3] and urban [20] particle size measurements adequately. In addition, particle size distributions can be well-represented by combinations of lognormal distributions [21]. The number of particles per logarithmic radius interval is given by:

$$\frac{dN}{d \ln r} = \frac{1}{\sqrt{2\pi} \ln \sigma_g} \exp \left\{ -\frac{1}{2} \cdot \left[ \frac{\ln(r/r_g)}{\ln \sigma_g} \right]^2 \right\} \quad (2)$$

where  $r_g$  is the geometric mean radius and  $\sigma_g$  is the geometric standard deviation.

Refractive index values were chosen to span those of the more commonly found atmospheric constituents, which are shown in table 1 for visible through middle-infrared wavelength regimes. The maximum values in the 0.55- to 1.06-micrometer and 3- to 5-micrometer bands are attributed to carbon particles [22,23], while the extreme values in the 9- to 11-micrometer band are due to quartz [24]. A somewhat wider range of refractive index values was adopted in this work to allow for possible extreme variations for the many constituents whose indexes are not yet measured.

#### EXTINCTION COEFFICIENT AS A FUNCTION OF REAL AND IMAGINARY INDEX OF REFRACTION

For sake of comparison, extinction and absorption coefficients are presented for a somewhat arbitrary aerosol mass loading of  $100\mu\text{g}/\text{m}^3$  and density of  $2.5\text{ g}/\text{cm}^3$ , roughly corresponding to a "light" aerosol mass loading equivalent to an approximate rural, maritime, or desert aerosol (under moderate wind conditions). Although calculations have been performed at wavelengths 0.55, 1.06, 3.8, 9.3, and 10.6 micrometers, results will mainly be presented for 0.55 micrometers, which broadly represents the visible to near-infrared regime, and for 10.6 micrometers, which is taken to represent approximately the 9- to 12-micrometer spectral range.

It is important to note that all results (with the exception of the bimodal distribution work discussed later) presented here are for a normalized mass of  $100\mu\text{g m}^{-3}$ . The mass,  $M$ , of a size distribution of particles characterized by the lognormal distribution is given by

$$M = 4\pi/3 N r_g^3 \exp(4.5 \ln^2 \sigma_g) \rho \quad (3)$$

where  $\rho$  is the particle density.

Thus, the results can be applied to a wide range of atmospheric conditions varying from a background or "light" aerosol loading to a "heavy" aerosol loading produced, for example, by a blowing dust, vehicular dust, or battlefield debris--providing the size distribution and mass of the aerosol particulates are adequately known.

The effects of real and imaginary index variations on extinction at these two wavelengths for a wide range of size distribution parameters are shown in fig 1 through 8. Changes in extinction by as much as a factor of 10 to 20 are caused by real or imaginary index variations at 10.6 micrometers (fig 1, 3, 5, 6, 7); whereas, except for distributions of predominately submicrometer particles, changes in extinction at 0.55 micrometer caused

by variations in real and imaginary indexes are less than 20 percent. A comparison between the effects of real and imaginary indexes on extinction is shown in fig 9.

To demonstrate the utility of these curves, consider the following example: Suppose there is a polydisperse aerosol characterized by lognormal parameters  $r_g = 0.1\mu\text{m}$ , and  $\sigma_g = 2.0$ , a mass loading of  $100\mu\text{g m}^{-3}$  and particle density  $2.5\text{g cm}^{-3}$ . Further, suppose the imaginary index of the aerosol at  $\lambda = 10.6\mu\text{m}$  is 0.25; then changes in real index from 1.2 to 3.5 cause changes in extinction coefficient from  $9.9 \times 10^{-3} \text{ km}^{-1}$  to  $3.3 \times 10^{-3} \text{ km}^{-1}$  (fig 1). Similarly, for the same size distribution of particles having real index 1.8 at  $\lambda = 10.6\mu\text{m}$ , changes in imaginary index from 0.05 to 1.0 result in extinction coefficient changes from  $1.6 \times 10^{-3} \text{ km}^{-1}$  to  $2.5 \times 10^{-2} \text{ km}^{-1}$  (fig 5). Again, although the calculations are only for 0.55- and 10.6-micrometer wavelengths, the range of complex indexes represents the entire visible to near infrared and 9- to 11-micrometer spectral regions.

Some of the tabulated results are presented here as a function of the parameter  $r_g/\lambda$  (geometric mean radius/wavelength). This parameter  $r_g/\lambda$  has no physical meaning as such and is merely used for the convenience of the reader who wishes to examine the effect of both the real and imaginary index in terms of the lognormal size distribution parameter  $r_g$  at selected wavelengths  $\lambda$ , at only the specific  $r_g/\lambda$  values given.

The effect of real index on extinction is generalized in table 2 where the ratio of extinction coefficient at real index  $n$  compared to the value at  $n = 1.33$  is tabulated as a function of  $r_g/\lambda$  values from 0.01 up to 1.0, for values of  $\sigma_g$  of 1.5, 2.0, and 2.5 for imaginary index value of 0.05. The real index has greatest effect for the narrower distributions and for  $r_g/\lambda \lesssim 0.25$ , where extinction can vary by up to a factor of about 20 with change in real index. However, extinction is relatively insensitive (within a factor of 3 and 30 percent for  $\sigma_g = 1.5$  and  $\geq 2.0$ , respectively) to variation in real indexes for  $r_g/\lambda \geq 0.25$ .

The effect of imaginary index on extinction is generalized in table 3 where extinction at imaginary index  $k$  is compared to the value of 0.05 for a range of  $r_g/\lambda$  values from 0.01 to 1.0 for real index equal to 1.6.

Briefly, extinction is invariant to imaginary indexes (to within  $\pm 20$  percent), and independent of particle size distribution spread, for  $r_g/\lambda \gtrsim 0.25$ . Extinction is independent (to within  $\pm 14$  percent) of imaginary indexes for  $k \lesssim 1.0$  for  $\sigma_g \geq 2.0$  and  $r_g/\lambda \geq 0.1$ . Variation in extinction by up to a factor of 20 is caused by changes in imaginary index for  $r_g/\lambda \lesssim 0.1$ , though these large variations decrease with increasing distribution spread.

## ABSORPTION COEFFICIENT AS A FUNCTION OF THE IMAGINARY AND REAL INDEX OF REFRACTION

The absorption coefficient is a linear function of imaginary index of refraction for a medium with homogeneous optical properties as expressed by the well-known Lambert absorption law. Use has been made of this law by several workers including Volz [25,26], Fischer [27], and Schleusener et al. [28] to infer values of imaginary index from bulk absorption coefficients. This approach may well introduce errors for absorbing constituents which do not possess uniform properties and which do not constitute all of the bulk material. Some of the associated problems were first pointed out by Bergstrom [29] and more recently by Toon et al. [6]. Waggoner et al. [30] showed that the absorption coefficient is linearly dependent to within a factor of 2 on imaginary index for  $k \leq 0.05$  and size parameter  $x$  ( $x = 2\pi r/\lambda$  where  $r$  is the particle radius and  $\lambda$  is the radiation wavelength) is  $\leq 8$ . However, many atmospheric constituents possess  $k$  values in excess of 0.05 particularly in the middle-infrared. For example, the departure from linearity of absorption coefficient versus  $k$  was noted by Bergstrom [29] for carbon particles ( $k = 0.66$ ). Another purpose of this report is to illustrate some of the problems associated with inferring imaginary index from absorption coefficients measured in a nonhomogeneous medium.

Figures 10 through 13 illustrate the effect of imaginary indexes on the absorption coefficient at wavelengths 0.55 and 10.6 micrometers for typical particle size distribution with geometric mean radius  $r_g$  of 0.1, 0.25, 0.5, and 1.0 micrometers with geometric standard deviation  $\sigma_g$  varying from 1.5 to 2.5. It is evident that absorption is no longer linearly dependent on imaginary index for increasing values of  $\sigma_g$ . This non-linear behavior results in a lower absorption than predicted by the Lambert absorption law.

Figure 14 shows a similar effect for wavelength 3.8 micrometers. For broad distributions the absorption coefficient is not linear with imaginary index, so that inference of imaginary index from the measurement of aerosol absorption, as done by Volz [25,26] and Schleusener et al. [28] should be viewed with skepticism, particularly for the middle-infrared spectral region. This point has also been raised by Toon et al. [6].

The values of imaginary index  $k_0$  below which the absorption coefficient varies linearly with imaginary index are shown in tables 4 and 5 for wavelengths 3.8, and 10.6 micrometers, respectively. The tables show that as the particle size distribution becomes broader, the range of  $k$  over which absorption is linear becomes narrower. Values of imaginary index below which the absorption coefficient varies linearly (within 20 percent) with imaginary index is shown in generalized form in table 6.

Values of imaginary index  $k_c$  above which the absorption is constant (within  $\pm 40$  percent) with imaginary index are shown in tables 7 and 8 for wavelengths 3.8 and 10.6 micrometers, respectively. The majority of  $k_c$  values for 3.8 micrometers wavelength are in excess of typical values of imaginary index measured in this wavelength regime. However, at 10.6 micrometers wavelength, values of  $k_c$  lie within realistic values of  $k$  at this wavelength, particularly for the broader particle size distributions ( $r_g \gtrsim 0.25$ ,  $\sigma_g \gtrsim 2.0$ ). Thus, a measurement of absorption does not uniquely determine the imaginary index for a broad distribution, even if the particle size distribution and real index are known.

Values of  $k$  above which the absorption coefficient is constant (to within  $\pm 40$  percent) with imaginary index are shown in table 9 for real index = 1.8. Note that the absorption becomes relatively insensitive to  $k$  at realistically low values of  $k$  (particularly for the 8- to 12-micrometer region) for the two broadest distributions, for  $r_g/\lambda \gtrsim 0.1$ . This insensitivity will also apply to highly absorptive constituents such as carbon in the visible to near-infrared regime.

The effect of imaginary indexes on absorption is shown in generalized form in table 10 where the ratio of the volume absorption coefficient at imaginary index  $k$  is compared to  $k = 0.05$  for real index  $n = 1.6$ . The table shows that for the narrowest distributions (for  $\sigma_g = 1.5$ ) the absorption is linear with imaginary index up to  $k = 1.0$  for  $r_g/\lambda \gtrsim 0.05$ . In addition, the absorption does not vary by more than a factor of about 2 for  $k \gtrsim 0.025$ , irrespective of distribution spread for  $r_g/\lambda \gtrsim 0.25$ .

The effect of real index on absorption is shown in fig 15 through 18 for realistic size distribution parameters and for  $\lambda = 0.55\mu\text{m}$  and  $10.6\mu\text{m}$ . A comparison of the effects of the real and imaginary index on absorption is shown in fig 19. The influence of real index on absorption is reduced for decreasing wavelength as shown in fig 20 for  $\lambda = 3.8\mu\text{m}$  and as also evidenced in fig 15 through 18.

Ratios of absorption for a range of real index values are shown in tables 11 and 12 for  $\lambda = 3.8\mu\text{m}$  and  $10.6\mu\text{m}$ . A generalized analysis of the effect of real index on absorption is summarized in table 13 where the absorption coefficient at real index  $n$  is compared to the value at  $n = 1.33$ . In general, the absorption does not vary by more than a factor of about 2 with the exception of the larger real index values at the lower values of  $r_g/\lambda$ .

The effects of real and imaginary index variations on both extinction and absorption at  $\lambda = 10.6\mu\text{m}$  are in general severely affected by the form of the size distribution as seen in fig 1 through 20. An exception can be seen in fig 10. In this case, variation of absorption coefficient with imaginary index is relatively unaffected by changes in size distribution parameters. In contrast to the results at  $\lambda = 10.6\mu\text{m}$ , at  $\lambda = 0.55\mu\text{m}$ , the effects of complex index variations are not greatly affected by changes of the size distribution parameters. The prime reason for the strong dependence of extinction and absorption on refractive indexes in the middle-infrared as compared to visible wavelengths is that the range of both real and imaginary indexes is much greater in the middle-infrared than in the visible. For broad distributions, the dependence of extinction and absorption on refractive indexes is reduced throughout this spectral range.

### Isoabsorption Analysis

Isoabsorption analyses were performed for several values of absorption coefficient which were normalized to a mass loading of  $100\mu\text{g m}^{-3}$  for wavelengths  $10.6\mu\text{m}$  and  $3.8\mu\text{m}$ . Some sample results are shown in fig 21 and 22 at  $\lambda = 10.6\mu\text{m}$  for  $r_g = 1.0\mu\text{m}$  and  $10\mu\text{m}$  and  $\sigma_g = 1.5$ . Here isoabsorption curves are drawn for three widely different absorption values (each normalized to  $100\mu\text{g m}^{-3}$ ) of  $3 \times 10^{-4} \text{ km}^{-1}$ ,  $2.4 \times 10^{-3} \text{ km}^{-1}$ , and  $1.75 \times 10^{-2} \text{ km}^{-1}$ . The isoabsorption values are kept constant to within  $\pm 15$  percent. A conclusion from these results is that in some cases variations of over two orders of magnitude in imaginary index of refraction can occur for a variation in real index from 0.1 to 8.0. In addition, for some absorption values two values of imaginary index are possible for a single real index value. The results of the isoabsorption analysis are summarized in tables 14 and 15 for wavelengths 10.6 and 3.8 micrometers for a wide range of particle size distributions. The uncertainty in imaginary indexes is considerably reduced by decreasing the range of real index. The analysis for  $\lambda = 3.8\mu\text{m}$  in table 15 shows that over a wide variation in particle size distribution parameters ( $r_g$  and  $\sigma_g$  varying from  $0.1\mu\text{m}$  to  $1.0\mu\text{m}$  with  $\sigma_g$  varying from 1.5 to 2.25), and for a possible uncertainty in real index values from 1.2 to 3.0, the ratio of imaginary index from minimum to maximum value can attain a factor of 5. If the uncertainty in real index is from 1.2 to 2.0, this factor is reduced to 3.5.

A similar analysis conducted for  $\lambda = 0.55\mu\text{m}$  indicated that over realistic values of particle size distribution parameters ( $r_g$  from  $0.1\mu\text{m}$  to  $1.0\mu\text{m}$ , and  $\sigma_g$  varying from 1.5 to 2.25), uncertainty in imaginary index by up to a factor of 3.0 is caused for a range of real index from 1.33 to 2.1. If the range is reduced to 1.7, the uncertainty factor is reduced to a maximum value of 1.6.

A comparison for two isoabsorption values of  $2.0 \times 10^{-4}$  and  $1.6 \times 10^{-3} \text{ km}^{-1}$  for the three size distributions of geometric mean radii of  $0.1\mu\text{m}$ ,  $1.0\mu\text{m}$ , and  $10.0\mu\text{m}$  is shown in table 16 for  $\lambda = 10.6\mu\text{m}$ . The results imply that, for the same variation in real index, significantly different ranges of imaginary index are obtained for the different size distributions. This implies that knowledge of the size distribution is imperative to accurately infer the values of the imaginary index from absorption measurements. In addition, knowledge of the real index is also necessary to evaluate the imaginary index, without which errors by more than an order of magnitude can occur in the interpolation of imaginary index even with a knowledge of the particle size distribution.

### Extinction and Absorption as a Function of Particle Size Distribution

Some results have already been presented on extinction as a function of particle size [31,32]. However, the analysis was limited to an upper limit of 2.0 for  $\sigma_g$ . In addition, no results were previously presented for absorption. Sample results are shown in fig 23 for  $\lambda = 0.55\mu\text{m}$  and  $10.6\mu\text{m}$  for extinction and absorption as a function of  $r_g$ . Inferred extinction values differ by more than an order of magnitude. Distributions having  $0.02 \lesssim r_g \lesssim 0.2\mu\text{m}$  at  $0.55\mu\text{m}$  wavelength and  $0.2 \lesssim r_g \lesssim 2\mu\text{m}$  at  $10.6\mu\text{m}$  yield maximum extinction values. For values of  $r_g/\lambda \gtrsim 0.5$ , Jennings and Gillespie [32] have shown that the extinction coefficient  $\sigma_e$  has the dependence  $\sigma_e \sim 1/r_g \exp(-2.5 \ln^2 \sigma_g)$ .

The effect of geometric mean radius upon the absorption coefficient is shown in fig 24 for  $3.8\mu\text{m}$  wavelength. Absorption is constant to within a factor of 3 for  $r_g \lesssim 1.5\mu\text{m}$ ,  $0.4\mu\text{m}$  for  $k = 0.025$  and  $0.25$ , respectively, for  $\lambda = 3.8\mu\text{m}$ . For wavelength of  $10.6\mu\text{m}$ , absorption is constant to within a factor of 3 for  $r_g \lesssim 1.7\mu\text{m}$ ,  $1.2\mu\text{m}$ , and  $0.8\mu\text{m}$  for  $k = 0.1$ ,  $0.25$ , and  $0.5$ , respectively. Absorption varies approximately as  $1/r_g$  for  $r_g \gtrsim 5.0\mu\text{m}$ ,  $3.5\mu\text{m}$ , and  $2.5\mu\text{m}$  for  $k = 0.1$ ,  $0.25$ , and  $0.5$ , respectively, for wavelength of  $10.6\mu\text{m}$ . Knowledge of the particle size distribution is very important in determining the value of the absorption for geometric mean radii in excess of a few micrometers.

The ratio of absorption to extinction for a wide range of realistic particle size distributions is shown in table 17 as imaginary index is varied from 0.005 up to 1.0. Three wavelengths of 0.694, 3.8, and 10.6 micrometers were used. Absorption constitutes about 50 percent of the extinction for  $r_g \gtrsim 1.0\mu\text{m}$  for the majority of imaginary index values.

## The Spectral Dependence of Extinction and Absorption

The effect of wavelength on the extinction coefficient is first examined for unimodal distributions. Particle size distributions with  $r_g = 0.1$ , 0.5, and 1.0 micrometers were chosen. Real index values of 1.6, 1.6, 1.5, and 1.8 and imaginary index values of 0.01, 0.01, 0.025, and 0.5 were assigned to wavelengths 0.55, 1.06, 3.8, and 10.6 micrometers, respectively. The refractive index values were considered to realistically represent typical values of the atmospheric aerosol. The variation of extinction with wavelength for narrow distributions ( $\sigma_g = 1.5$ ) is shown in fig 25(a).

One sees a gradual transition from a strong dependence of extinction on wavelength ( $\lambda^{-2.5}$  up to  $3.8\mu\text{m}$ ) to almost neutral extinction for  $r_g = 1\mu\text{m}$ . Similar plots are drawn in fig 25(b) for broader distributions ( $\sigma_g = 2.5$ ), for the same  $r_g$  values as in fig 25(a). The figure shows that the extinction is neutral with respect to wavelength for the two larger  $r_g$  values. It should be noted that any inferences made between extinction and wavelength from this figure are only valid at the discrete wavelengths used.

To demonstrate the spectral dependence of extinction for a range of refractive index values, the authors have chosen to limit this study to desert aerosols. Two bimodal distributions representative of measurements by Sverdrup et al. [33], Patterson and Gillette [3], Junge and Jaenicke [34], and De Luisi et al. [35] have been constructed for this spectral study, referred to here as "light" and "heavy" aerosol loadings. The parameters for these distributions appear in table 18. Desert aerosols are known [1,4,36] to contain quartz, montmorillonite, kaolinite, illite, calcite, sodium nitrate, ammonium sulfate, and carbon; therefore the range of extinction coefficients resulting from variation of refractive indexes over the gamut of values measured for the majority of these constituents has been determined for the visible, 3 to 5 micrometers, and 9 to 11 micrometers spectral regions.

Ammonium sulfate and carbon have been assumed to be present only in the small particle mode of the "light" aerosol, consistent with findings of Blanco and McIntyre [2], Lindberg and Gillespie [4], and Cartwright et al. [7]. Typical and extreme of index values are taken (or estimated, in the case of typical values) from the works of Fischer [37,38], Lindberg and Laude [39], Toon et al. [5,6], Spitzer and Kleinman [24], Hänel [40], Foster and Howarth [23], Dalzell and Sarofim [22], Querry et al. [41], Downing et al. [42], and Grams et al. [43]. The resulting spectral variations due to these refractive index variations are shown in fig 26; the circles mark the extinction values corresponding to the typical refractive indexes, and the minimum and maximum values of extinction obtained are indicated by the "error" bars. Values of complex refractive indexes giving minimum and maximum extinction are given in table 19; also given are the typical index values. For example, at 10.6 micrometers, minimum extinction for the "light" aerosol loading is obtained with a combination of ammonium sulfate ( $m = 1.99 - 0.06 i$ ) and sodium nitrate ( $m = 1.19 - 0.07 i$ ) for the small and large particle modes; and the maximum extinction from a

combination of carbon ( $m = 2.04 - 1.28 i$ ) and quartz ( $m = 2.18 - 0.02 i$ ) for the two modes. Variation in the complex refractive index causes only a small change in extinction (less than 15 percent), in agreement also with the work of Gillespie et al. [44]. For the "light" aerosol loading, extinction spectral dependence is very roughly  $1/\lambda$ , as variation in optical constants in the 4- to 10-micrometer wavelength regime results in significant (up to a factor of 10) extinction uncertainties. Neutral extinction prevails for the "heavy" aerosol loading, except for the 10-micrometer region where refractive index variations cause moderate (factor  $\sim 3$ ) uncertainties in extinction.

No results are presented here for "moderate" aerosol loadings typified by mass loadings in the order of  $5 \times 10^2$  to  $5 \times 10^3 \mu\text{g}/\text{m}^3$  and described by Patterson and Gillette [3]. However, an examination of typical size distribution parameters for these moderate aerosol conditions [3] indicates that the size distribution values roughly correspond to those of the heavy aerosol loading. Consequently, the same conclusions based on the heavy aerosol case will also approximately apply to the moderate aerosol case.

The values for extinction,  $\text{km}^{-1}$ , are given in table 20 for the small and large particle modes (parameter values given in table 18) for the "light" and "heavy" aerosol loadings. The corresponding complex refractive values appear in table 19. The use of table 20 allows one to examine the effect of the variation of loadings on extinction values.

Typical, minimum, and maximum absorption values corresponding to a gamut of complex refractive values shown in table 21 are given in table 22. The resulting absorption for both the "light" and "heavy" aerosol loadings is shown in fig 27. The figure shows that uncertainty in index of refraction values can cause at least an order of magnitude variation on absorption for both the "light" and "heavy" aerosol case. The larger degree of uncertainty as compared to the extinction case is primarily due to the strong dependence of absorption on imaginary index.

The reader is reminded that all results presented here are for polydispersions of spherical particles, and thus caution should be exercised in applying them to irregular particles. However, for particles large compared to the wavelength, Chylek [45] has shown that the extinction cross section of arbitrarily shaped randomly oriented irregular particles is always greater than the extinction cross section for a sphere of equal volume. Consequently, in the large particle limit, these results may be used as a lower bound for extinction by nonspherical particles of known volume. In the small particle limit, angular scattering measurements on slightly irregular particles by Pinnick et al. [46] and Zerull [47], and extinction efficiency measurements by Greenberg [48] suggest they may be approximated by spheres of equal area or volume, providing size parameters are less than 3. Hence, the results presented here might be applied to polydispersions of slightly irregular particles, providing those predominant in extinction have size parameters less than 3.

## CONCLUSIONS

The extinction coefficient of polydispersions of spherical aerosols with a fixed mass loading is independent of both real and imaginary index to within about 20 percent for the majority of realistic size distributions in the visible and near-infrared wavelength regime ( $0.55\mu\text{m} \leq \lambda \leq 1.06\mu\text{m}$ ).

In the middle-infrared ( $9.3\mu\text{m} \leq \lambda \leq 10.6\mu\text{m}$ ) extinction is more strongly dependent on refractive indexes, particularly the real index, as changes in extinction of up to an order of magnitude are caused by variation of real index over the gamut of realistic values. The prime reason for the strong dependence of extinction and absorption on refractive indexes in the middle-infrared as compared to visible wavelengths is that the range of both real and imaginary indexes is much greater in the middle-infrared than in the visible. The dependence of both extinction and absorption on optical constants is mitigated as the particle size distribution is broadened.

Absorption is not in general linear with imaginary index, especially for broad distributions of particles; consequently, a measurement of the absorption coefficient does not uniquely determine the imaginary index. In general, the size distribution and the real index of the particles must be known. Isoabsorption plots of imaginary index and real index strongly suggest that variations by over two orders of magnitude can occur in the imaginary index if the real index is unknown at  $10.6\mu\text{m}$ . However, if real index is uncertain over a more realistic range from 1.0 to 3.0 at  $\lambda = 10.6\mu\text{m}$ , the uncertainty in imaginary index is reduced to factors from between 3 to 5. An increase in particle size distribution spread tends to reduce the overall variation in imaginary index.

In the middle-infrared, real index significantly influences the absorption, and this influence is enhanced for distributions of predominately sub-micrometer particles. The dependence of extinction on particle size is mitigated as particles become more absorptive. Absorption is generally less dependent on size distribution than is extinction.

Neutral extinction results for a "heavy" aerosol loading characterized by a bimodal distribution, whereas an approximate  $1/\lambda$  wavelength dependence predominates for a "light" aerosol loading. Uncertainties by more than an order of magnitude occur in absorption for a similar analysis. Uncertainty in the values of optical constants can cause large deviations in calculated extinction and absorption in the middle-infrared, and this underlines the necessity of obtaining measurements of both real and imaginary indexes of more atmospheric constituents, such as kaolinite and illite, in this spectral range.

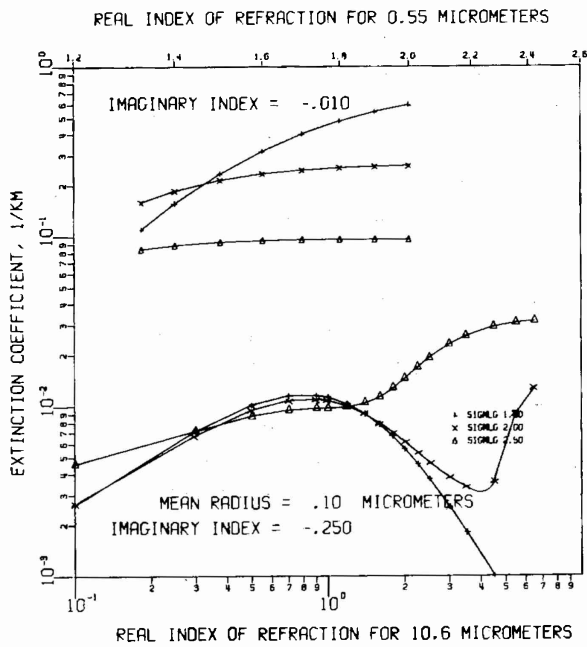


Figure 1

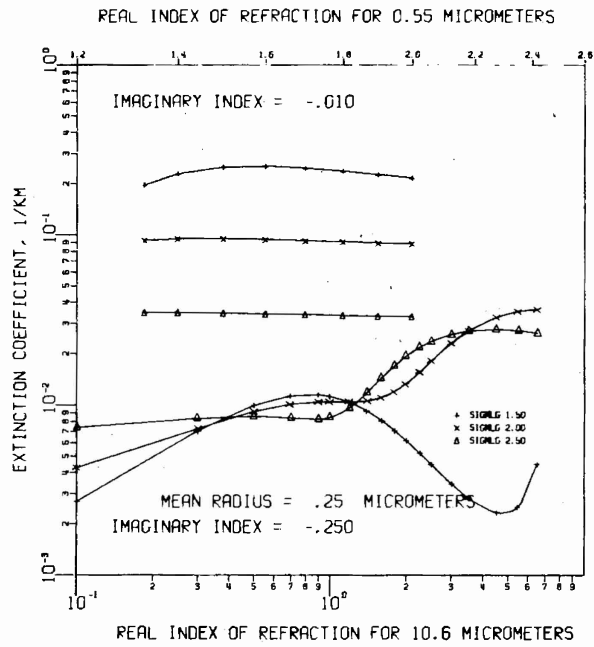


Figure 2

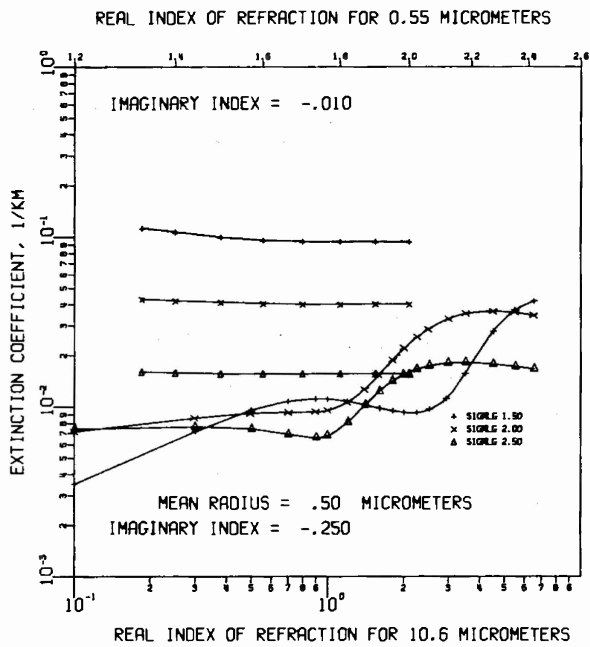


Figure 3

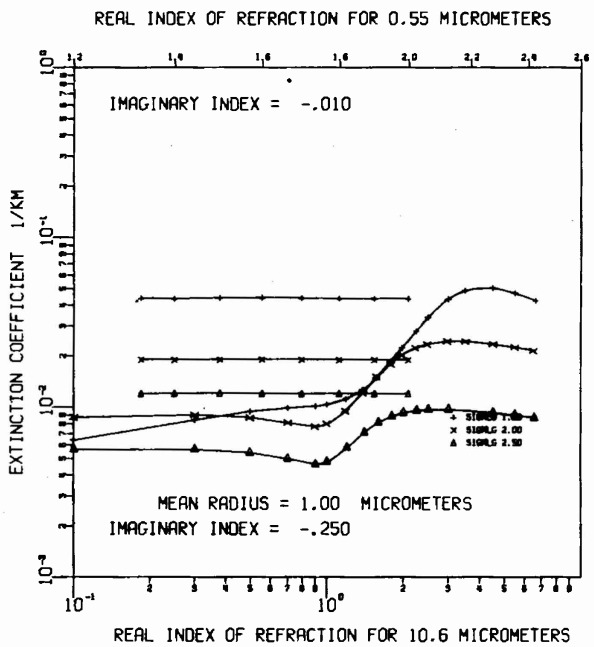


Figure 4

Figures 1 through 4. Extinction as a function of real index of refraction for wavelengths 0.55 $\mu\text{m}$  and 10.6 $\mu\text{m}$ . The mean denotes the geometric mean radius  $r_g$  and SIGMLG is the geometric standard deviation  $\sigma_g$ . The aerosol mass loading is 100 $\mu\text{g m}^{-3}$  for a particle density of 2.5  $\text{g cm}^{-3}$ .

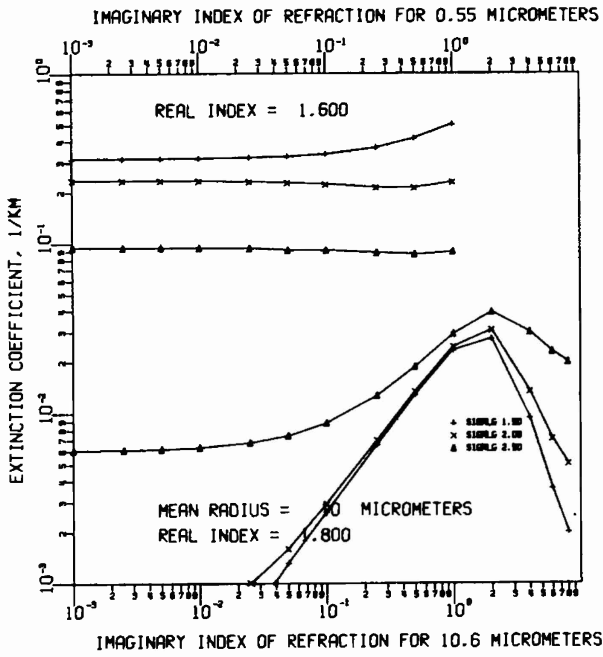


Figure 5

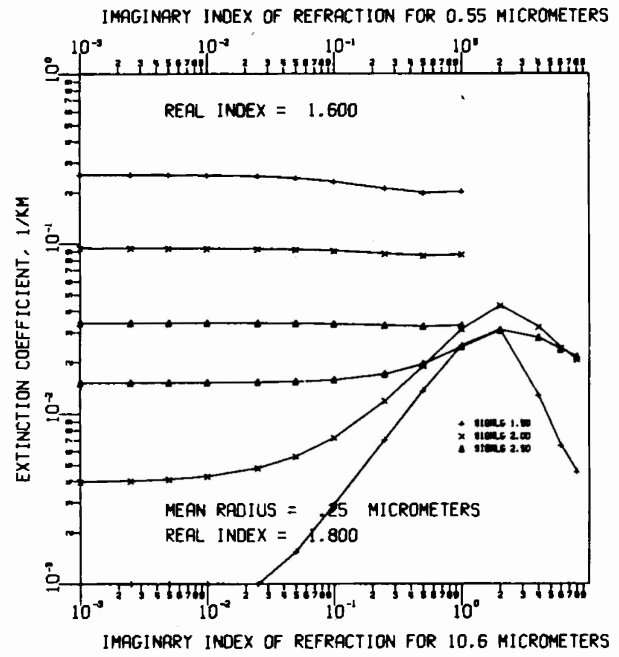


Figure 6

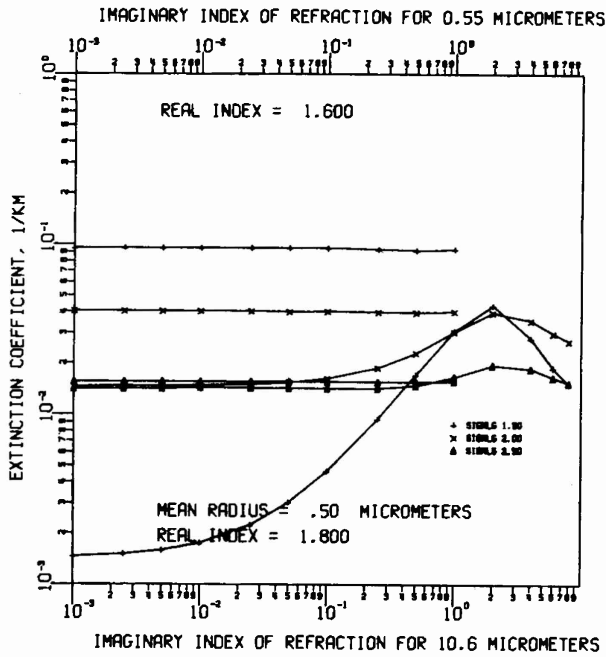


Figure 7

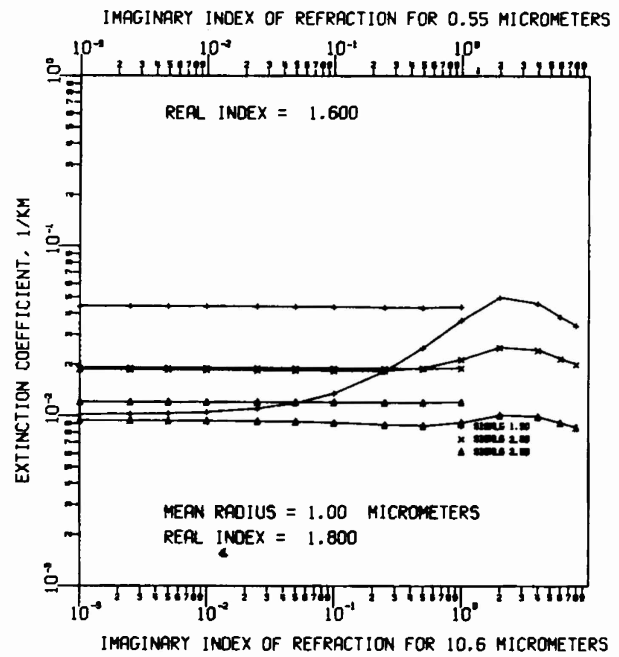


Figure 8

Figures 5 through 8. Extinction as a function of imaginary index of refraction for wavelengths  $0.55\mu\text{m}$  and  $10.6\mu\text{m}$ . The mean radius denotes the geometric mean radius  $r_g$  and SIGMLG is the geometric standard deviation  $\sigma_g$ . The aerosol mass loading is  $100\mu\text{g m}^{-3}$  for a particle density of  $2.5\text{ g cm}^{-3}$ .

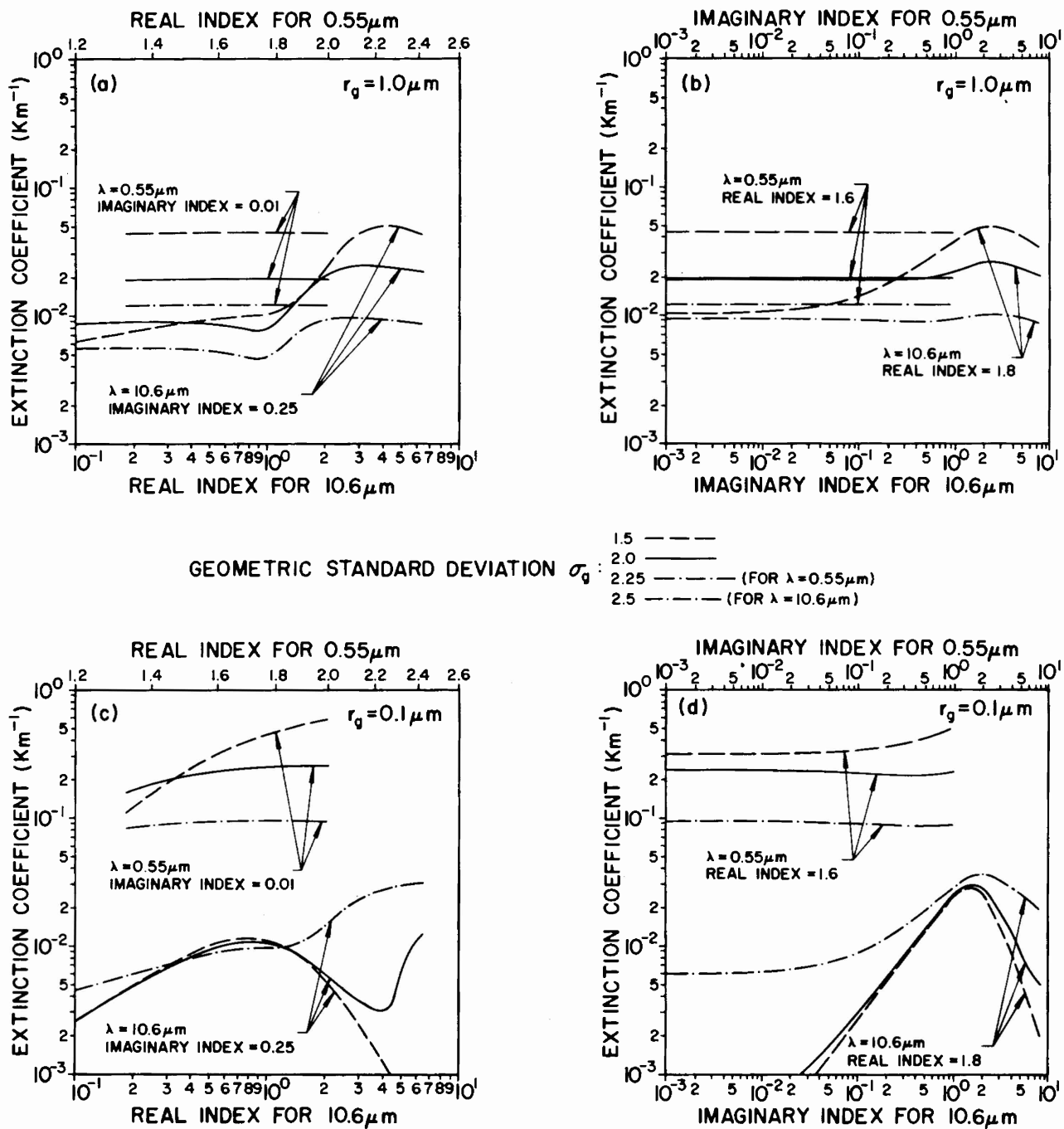


Figure 9. Aerosol extinction coefficient as a function of real and imaginary index of refraction for an aerosol mass loading of  $100 \mu\text{g m}^{-3}$  at  $0.55 \mu\text{m}$  and  $10.6 \mu\text{m}$  wavelength for a range of particle size distributions.

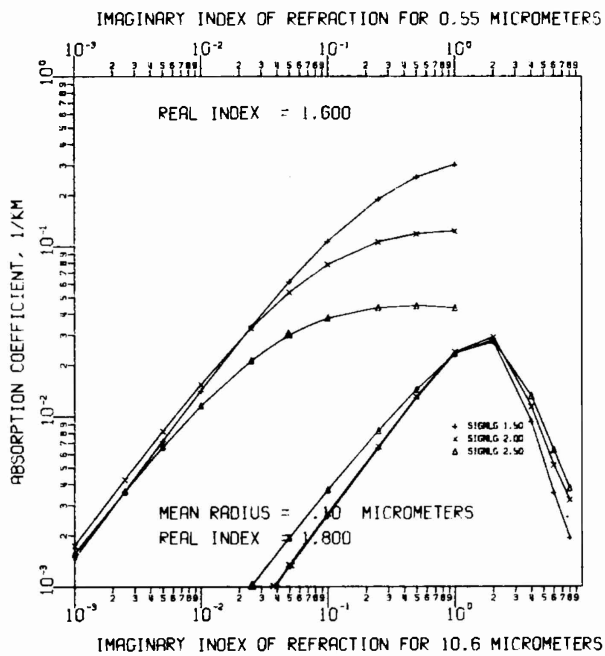


Figure 10

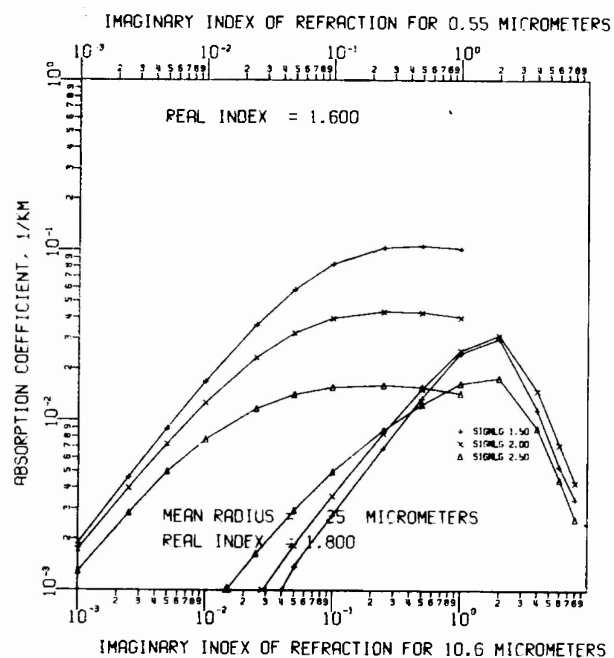


Figure 11

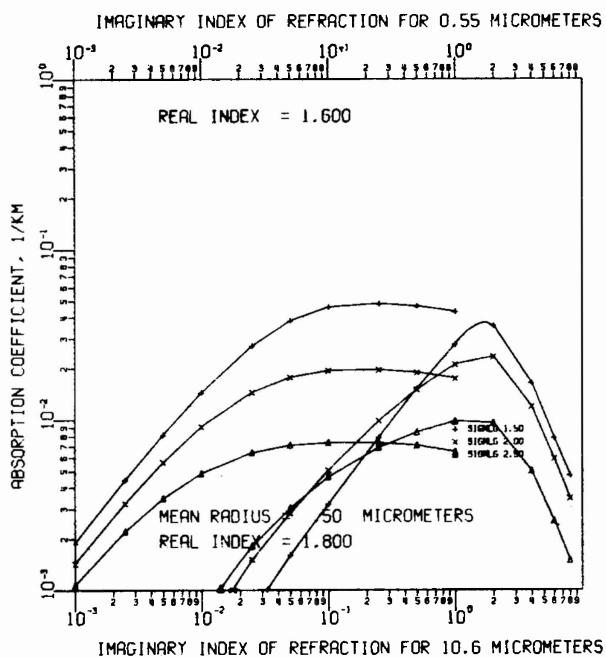


Figure 12

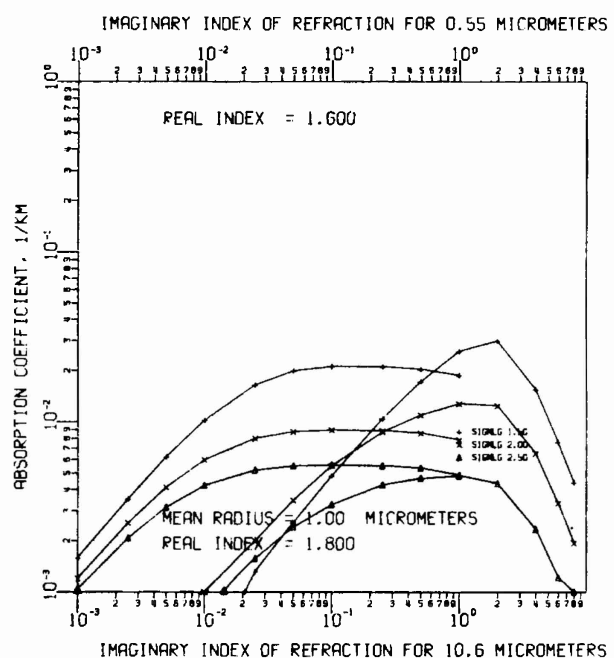


Figure 13

Figures 10 through 13. Absorption as a function of imaginary index of refraction for wavelengths  $0.55\mu\text{m}$  and  $10.6\mu\text{m}$ . The mean radius denotes the geometric mean radius  $r_g$  and SIGMLG is the geometric standard deviation  $\sigma_g$ . The aerosol mass loading is  $100\mu\text{g m}^{-3}$  for a particle density of  $2.5\text{ g cm}^{-3}$ .

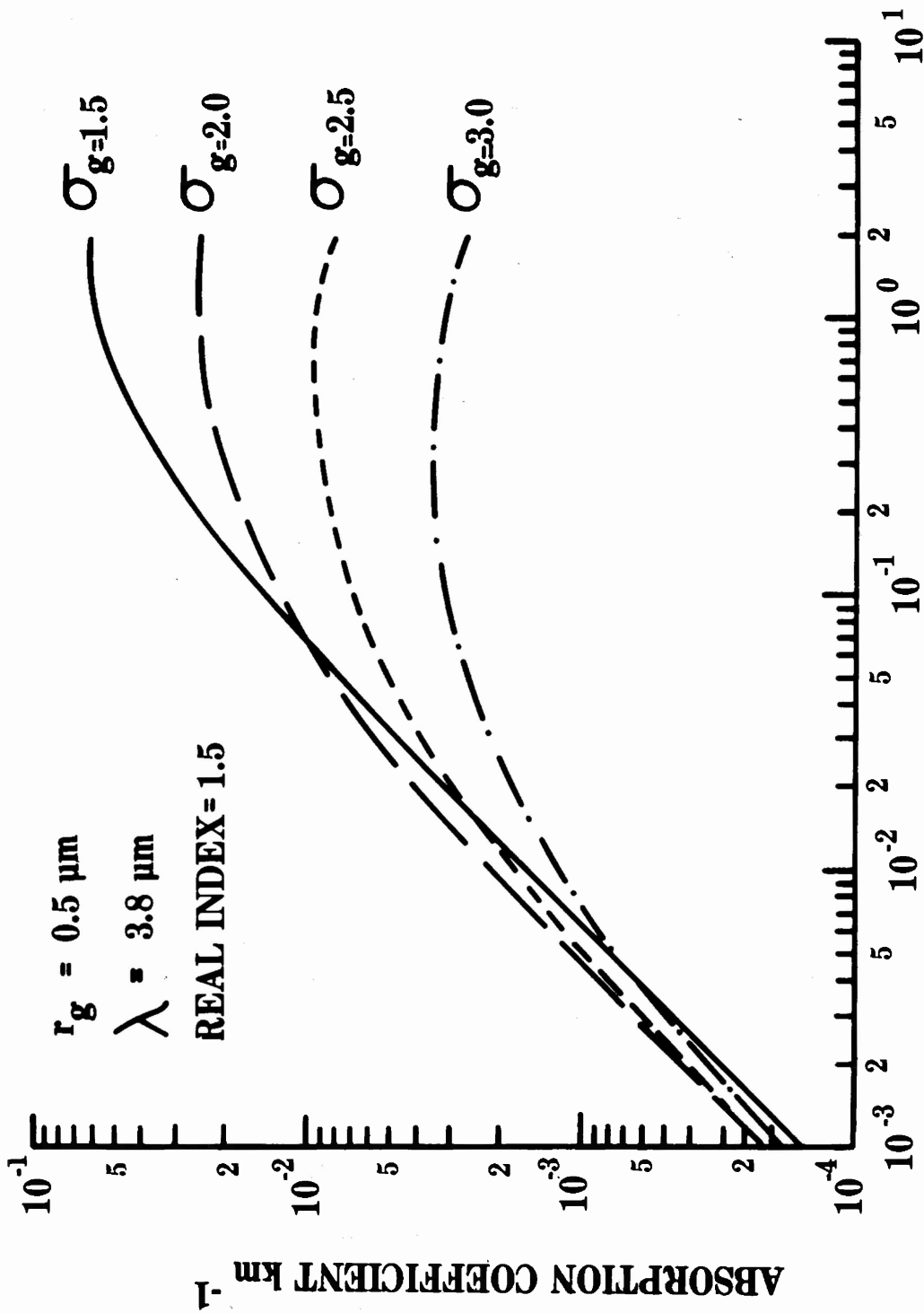
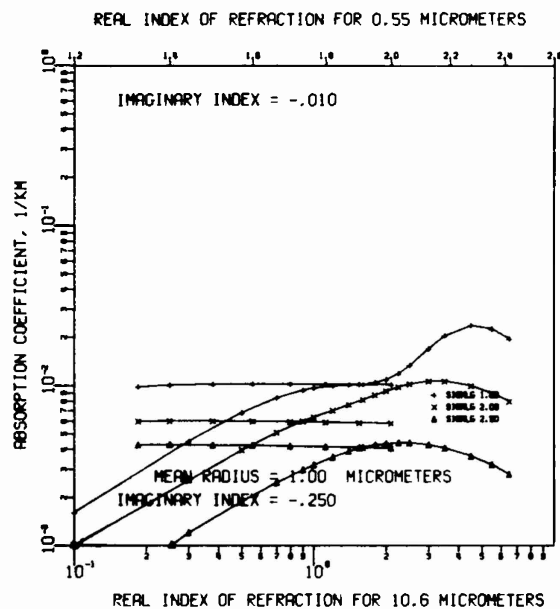
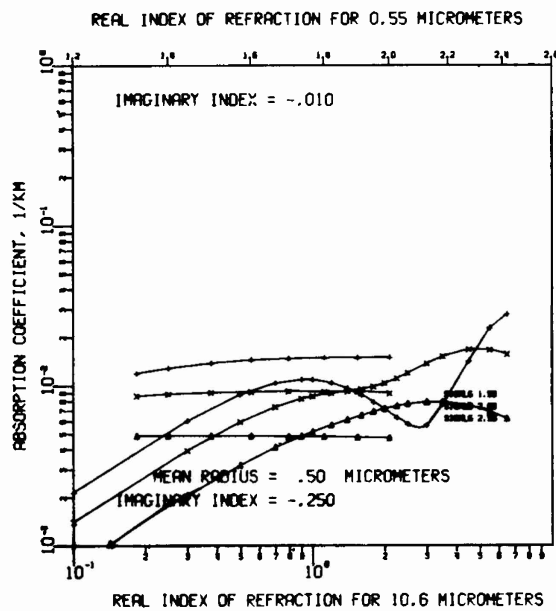
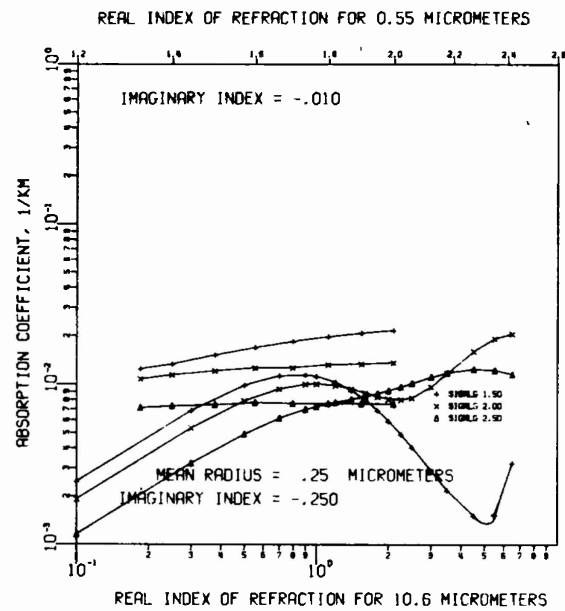
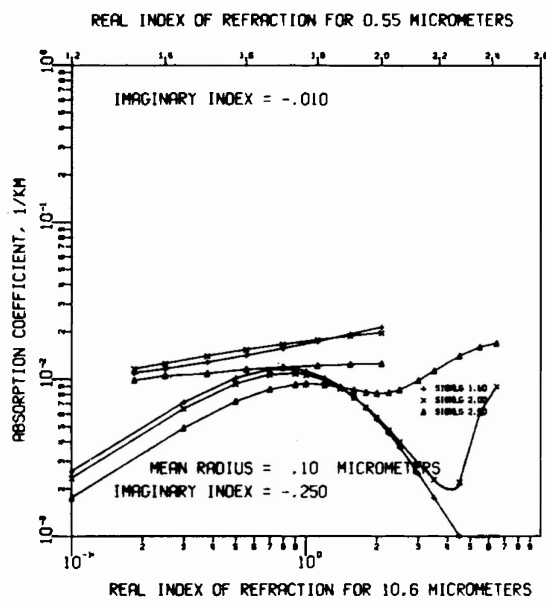


Figure 14. Absorption as a function of imaginary index of refraction for wavelength 3.8 $\mu\text{m}$ . Aerosol mass loading = 100 $\mu\text{g m}^{-3}$  and particle density = 2.5 g  $\text{cm}^{-3}$ .



Figures 15 through 18. Absorption as a function of real index of refraction for wavelengths  $0.55\mu\text{m}$  and  $10.6\mu\text{m}$ . The mean radius denotes the geometric mean radius  $r_g$  and SIGMLG is the geometric standard deviation  $\sigma_g$ . The aerosol mass loading is  $100\mu\text{g m}^{-3}$  for a particle density of  $2.5\text{ g cm}^{-3}$ .

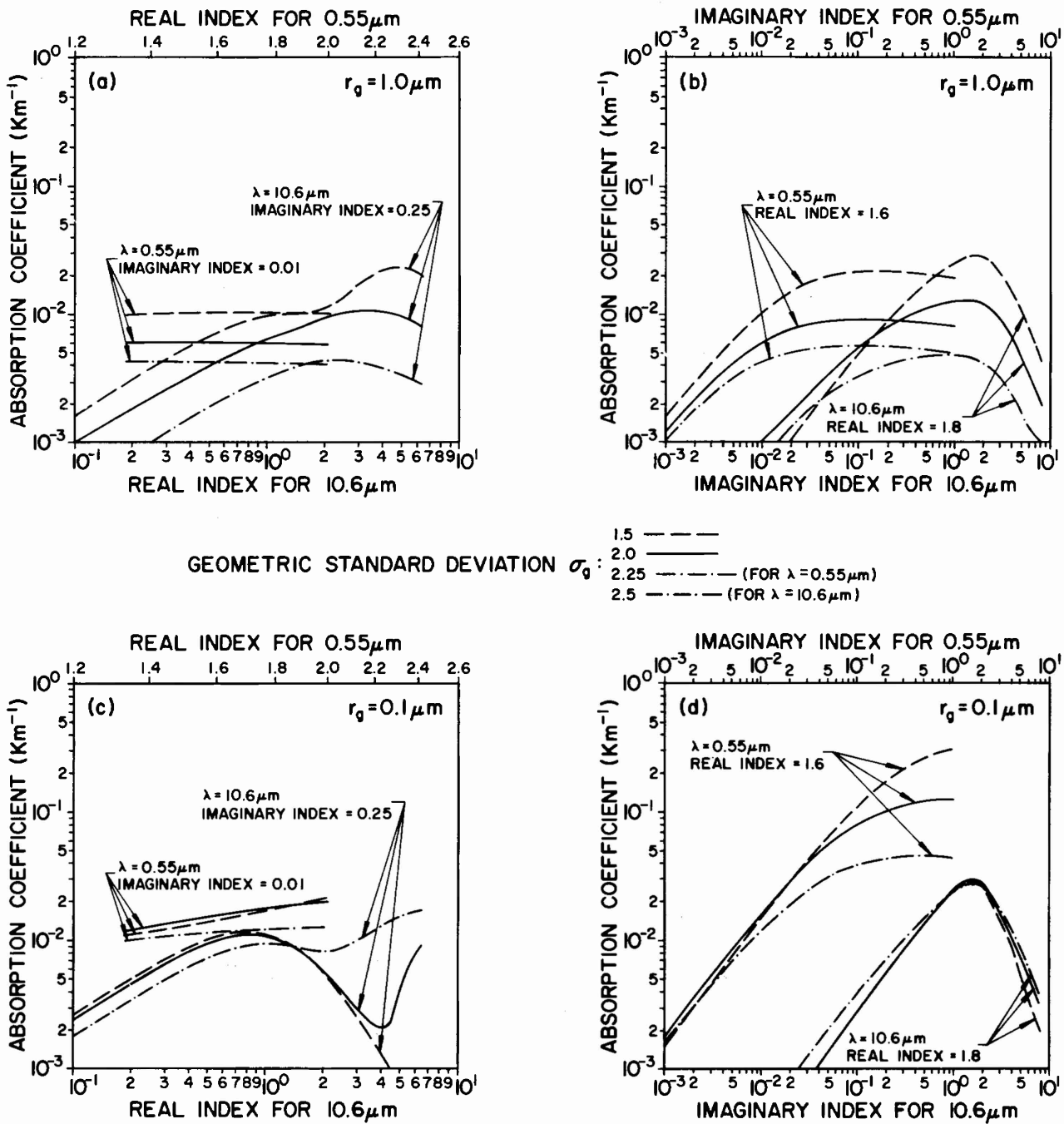


Figure 19. Aerosol absorption coefficient as a function of real and imaginary index of refraction for an aerosol mass loading of  $100\mu\text{g m}^{-3}$  at  $0.55\mu\text{m}$  and  $10.6\mu\text{m}$  wavelength for a range of particle size distributions.

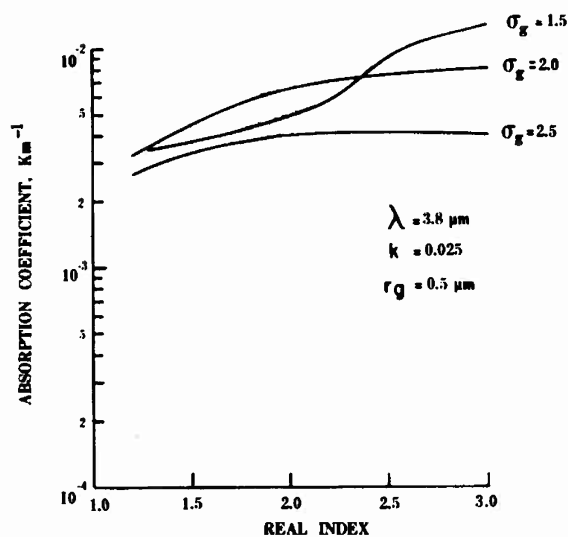


Figure 20. Absorption coefficient as a function of real index of refraction for an aerosol mass loading of  $100\mu\text{g m}^{-3}$  at wavelength  $3.8\mu\text{m}$ .

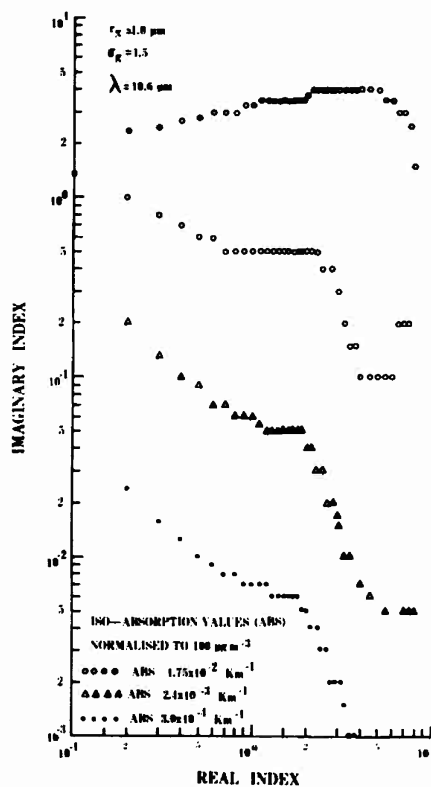


Figure 21. Isoabsorption curves for wavelength  $10.6\mu\text{m}$ . Aerosol mass loading =  $100\mu\text{g m}^{-3}$  and particle density =  $2.5\text{ g cm}^{-3}$ . The geometric mean radius,  $r_g = 1.0\mu\text{m}$  and geometric standard deviation = 1.5.

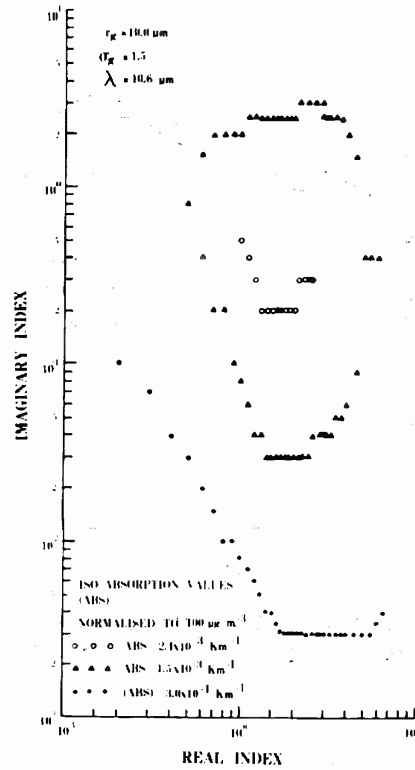


Figure 22. Isoabsorption curves for wavelength  $10.6\mu\text{m}$ . Aerosol mass loading =  $100\mu\text{g m}^{-3}$  and particle density =  $2.5\text{ g cm}^{-3}$ . The geometric mean radius,  $r_g = 10.0\mu\text{m}$  and geometric standard deviation =  $1.5$ .

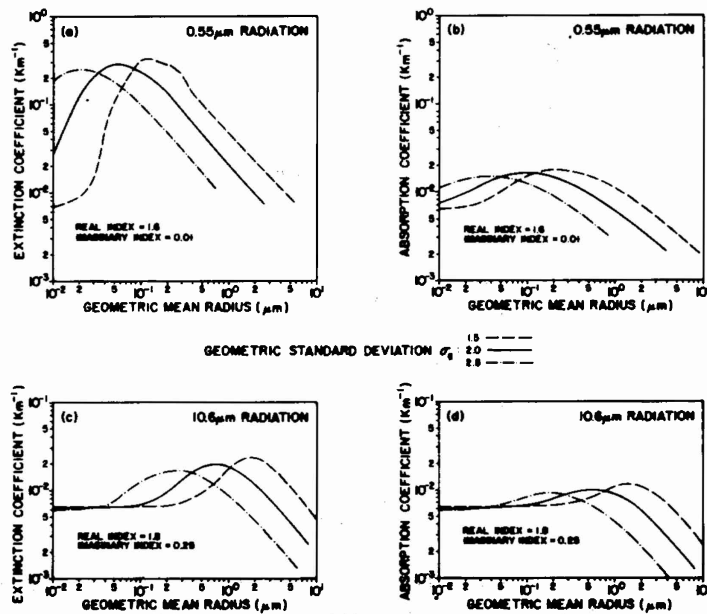


Figure 23. Aerosol extinction coefficient as a function of particle size distribution parameters (geometric mean radius and geometric standard deviation) for an aerosol mass loading of  $100\mu\text{g m}^{-3}$  at  $0.55\mu\text{m}$  and  $10.6\mu\text{m}$  wavelengths for selected complex refractive index values.

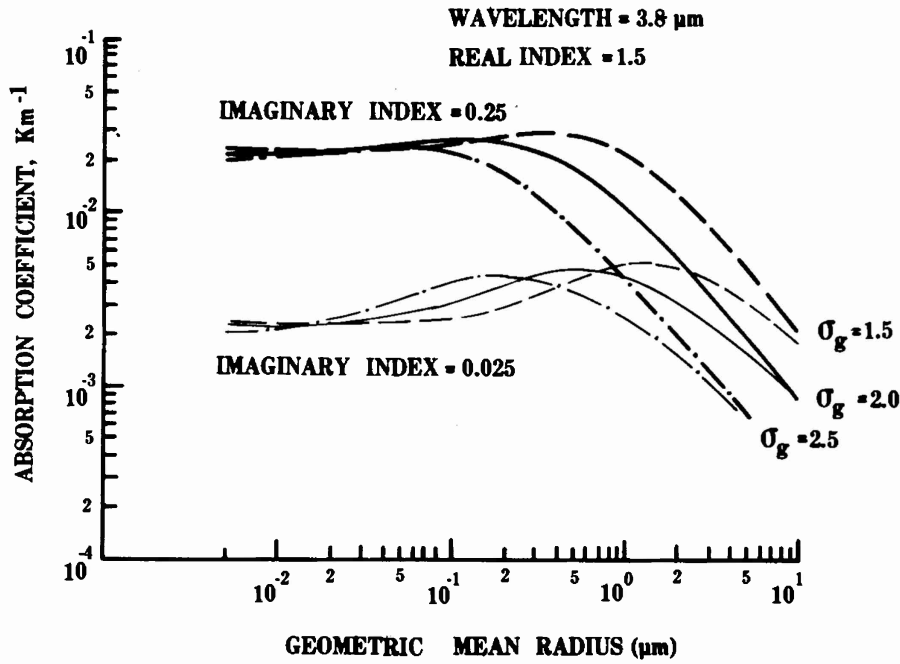


Figure 24. The absorption as a function of geometric mean radius for wavelength  $3.8\mu\text{m}$ . Real index = 1.5, for imaginary index values of 0.025 and 0.25.

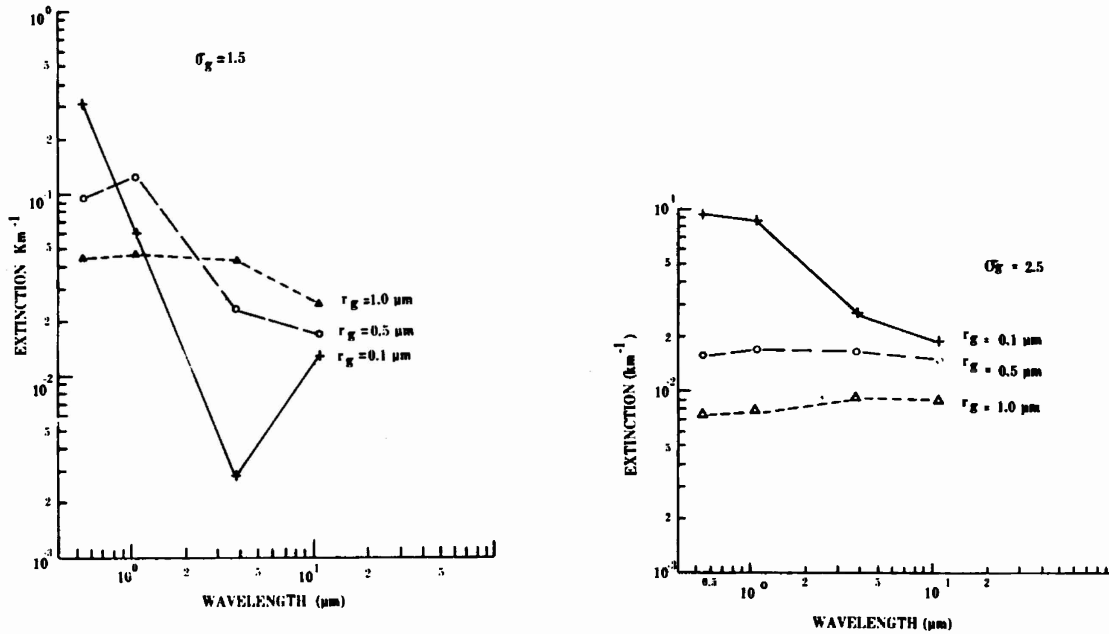


Figure 25. The variation of extinction with wavelength for narrow ( $\sigma_g = 1.5$ ) and broad ( $\sigma_g = 2.5$ ) unimodal distributions. Geometric mean radii of  $0.1\mu\text{m}$ ,  $0.5\mu\text{m}$  and  $1.0\mu\text{m}$  are used. Aerosol mass loading =  $100\mu\text{g m}^{-3}$  and particle density =  $2.5 \text{ g cm}^{-3}$ . Real index values of 1.6, 1.6, 1.5, and 1.8 and imaginary index values of 0.01, 0.01, 0.025 and 0.5 were assigned at wavelengths 0.55, 1.06, 3.8, and  $10.6\mu\text{m}$ .

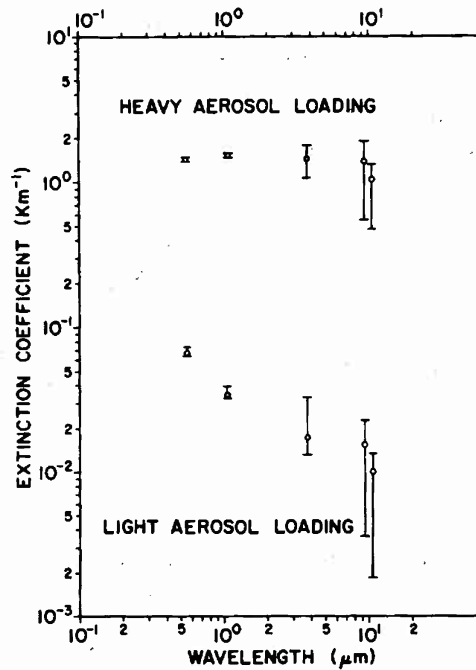


Figure 26. Aerosol extinction coefficient versus wavelength for light ( $60\mu\text{g m}^{-3}$ ) and heavy ( $1.5 \times 10^4\mu\text{g m}^{-3}$ ) bimodal particle size distributions (table 18). The circles indicate extinction values for typical refractive indexes (table 19) and the "error" bars indicate the extreme extinction values due to refractive index variations.

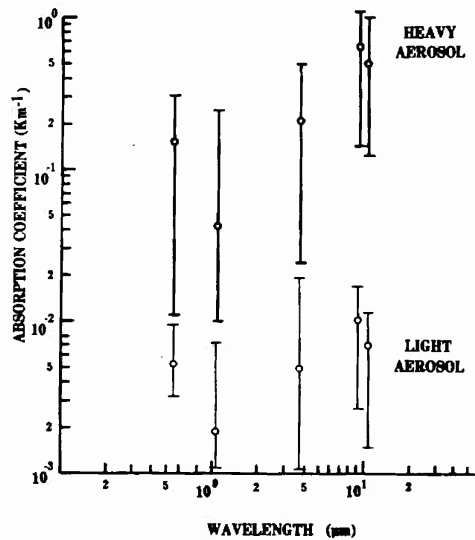


Figure 27. Aerosol absorption coefficient versus wavelength for light ( $60\mu\text{g m}^{-3}$ ) and heavy ( $1.5 \times 10^4\mu\text{g m}^{-3}$ ) bimodal particle size distributions (table 18). The circles indicate absorption values for typical refractive indexes (table 21) and the "error" bars indicate the extreme absorption values due to refractive index variations.

TABLE 1. RANGE OF MEASURED VALUES OF OPTICAL CONSTANTS OF SEVERAL ATMOSPHERIC CONSTITUENTS

Wavelength Range ( $\mu\text{m}$ )	Real Index	Imaginary Index
0.55 to 1.06	1.32 to 2.1	~ 0 to 0.8
3.0 to 5.0	1.2 to 3.1	~ 0 to 1.82
9.0 to 11.0	0.11 to 7.49	~ 0 to 7.51

TABLE 2. †VOLUME EXTINCTION COEFFICIENT AT REAL INDEX n  
VOLUME EXTINCTION COEFFICIENT AT REAL INDEX n = 1.33

Geometric Mean Radius, $r_{g/\lambda}$								
Wavelength	0.01	0.025	0.05	0.1	0.25	0.15	1.0	
Real Index n								
$\sigma_g = 1.5$	1.33	1.0	1.0	1.0	1.0	1.0	1.0	
	1.5	0.89	0.93	1.11	1.59	1.72	1.19	0.93
	1.7	0.77	0.85	1.30	2.60	2.40	1.16	0.90
	1.9	0.66	0.78	1.53	3.92	2.74	1.09	0.90
	2.2*	0.52	0.71	1.95	6.28	2.82	1.02	0.90
	2.5	0.41	0.66	2.44	8.64	2.68	1.00	0.89
	3.5	0.21	0.61	7.16	12.61	2.26	0.99	0.87
	5.0	0.11	0.68	16.28	11.75	2.17	0.95	0.85
	6.5	0.08	4.37	19.00	10.22	2.10	0.93	0.84
$\sigma_g = 2.0$	1.33	1.0	1.0	1.0	1.0	1.0	1.0	
	1.5	0.94	1.32	1.70	1.59	1.21	1.03	0.97
	1.7	0.89	1.88	2.70	2.12	1.30	1.00	0.96
	1.9	0.85	2.68	3.70	2.50	1.31	0.98	0.96
	2.2*	0.82	4.23	4.90	2.83	1.29	0.96	0.96
	2.5	0.82	5.89	5.76	2.98	1.26	0.95	0.95
	3.5	0.91	10.17	7.10	2.98	1.17	0.93	0.94
	5.0	4.17	12.90	7.14	2.76	1.13	0.91	0.93
	6.5	7.33	13.36	6.70	2.61	1.10	0.86	0.91
$\sigma_g = 2.5$	1.33	1.0	1.0	1.0	1.0	1.0	1.0	
	1.5	1.45	1.63	1.41	1.24	1.06	1.00	0.99
	1.7	2.21	2.31	1.77	1.38	1.08	0.98	0.99
	1.9	3.15	2.84	2.01	1.46	1.07	0.97	0.99
	2.2*	4.73	3.47	2.22	1.50	1.05	0.96	0.99
	2.5	6.10	3.89	2.33	1.50	1.06	0.96	0.98
	3.5	8.65	4.47	2.38	1.46	1.03	0.95	0.98
	5.0	10.24	4.48	2.27	1.38	0.97	0.93	0.97
	6.5	10.57	4.28	2.16	1.32	0.96	0.92	0.97

\* Applicable Only to Wavelengths  $> 2\mu\text{m}$  For  $n > 2.2$   
 †Imaginary Index  $k = 0.05$  For All Calculations

TABLE 3. VOLUME EXTINCTION COEFFICIENT AT IMAGINARY INDEX k  
 VOLUME EXTINCTION COEFFICIENT AT IMAGINARY INDEX k = 0.05

GEOMETRIC MEAN RADIUS $r_g$		0.01	0.025	0.05	0.1	0.25	0.5	1.0
WAVELENGTH $\lambda$								
Imaginary Index k								
$\sigma_g=1.5$	0.001	0.03	0.09	0.38	0.77	1.03	1.04	0.99
	0.0025	0.06	0.12	0.39	0.77	1.03	1.04	1.00
	0.005	0.11	0.17	0.43	0.78	1.03	1.04	1.00
	0.01	0.20	0.26	0.49	0.81	1.03	1.04	1.00
	0.025	0.50	0.54	0.68	0.88	1.01	1.02	1.00
	0.05	1.00	1.00	1.00	1.00	1.00	1.00	1.00
	0.10	1.99	1.93	1.63	1.23	0.98	0.96	1.00
	0.25	4.96	4.69	3.52	1.86	0.95	0.88	0.99
	0.50	9.80	9.22	6.59	2.78	0.96	0.83	0.98
	1.0	18.13	17.25	12.26	4.30	1.05	0.85	1.00
	2.0*	20.37	20.78	17.46	6.08	1.21	0.92	1.06
	4.0	5.95	7.49	10.61	5.50	1.17	0.90	1.05
6.0	2.20	3.73	7.15	4.58	1.06	0.83	0.99	
8.0	1.21	2.63	5.80	4.10	1.00	0.79	0.95	
$\sigma_g=2.0$	0.001	0.13	0.59	0.89	1.00	1.03	1.02	1.00
	0.0025	0.15	0.61	0.89	1.00	1.03	1.02	1.00
	0.005	0.20	0.63	0.90	1.00	1.03	1.01	1.00
	0.01	0.29	0.67	0.91	1.00	1.03	1.01	1.00
	0.025	0.56	0.79	0.94	1.00	1.02	1.01	1.00
	0.05	1.00	1.00	1.00	1.00	1.00	1.00	1.00
	0.10	1.89	1.41	1.11	1.00	0.96	0.99	1.00
	0.25	4.54	2.57	1.43	1.04	0.92	0.95	0.99
	0.50	8.89	4.40	1.90	1.14	0.90	0.93	0.99
	1.0	16.63	7.58	2.73	1.37	0.94	0.94	1.00
	2.0*	20.45	10.60	3.67	1.67	1.03	1.00	1.05
	4.0	7.94	7.54	3.21	1.59	1.00	0.99	1.06
6.0	4.14	5.68	2.69	1.42	0.93	0.94	1.01	
8.0	2.98	4.88	2.42	1.31	0.88	0.90	0.98	
$\sigma_g=2.5$	0.001	0.70	0.96	1.00	1.05	1.00	1.01	1.00
	0.0025	0.71	0.96	1.00	1.05	1.01	1.01	1.00
	0.005	0.73	0.96	1.00	1.05	1.01	1.01	1.00
	0.01	0.76	0.97	1.00	1.05	1.01	1.01	1.00
	0.025	0.85	0.98	1.00	1.04	1.01	1.00	1.02
	0.05	1.00	1.00	1.00	1.00	1.00	1.00	1.00
	0.10	1.29	1.05	1.01	1.01	0.98	0.99	1.00
	0.25	2.13	1.21	1.03	0.99	0.95	0.98	1.00
	0.50	3.42	1.49	1.12	0.99	0.93	0.97	1.00
	1.0	5.66	2.01	1.33	1.08	0.95	0.98	1.01
	2.0*	7.71	2.61	1.61	1.23	1.02	1.03	1.04
	4.0	5.58	2.29	1.51	1.19	1.01	1.03	1.05
6.0	4.28	1.94	1.34	1.09	0.95	0.99	-	
8.0	3.72	1.76	1.24	1.03	0.91	0.96	-	

\*Applicable only to wavelengths  $\geq 2 \mu\text{m}$  for  $k \leq 2.0$ .  
 (real index = 1.6)

TABLE 4. VALUES OF IMAGINARY INDEX  $k_{\ell}$  BELOW WHICH THE ABSORPTION COEFFICIENT VARIES LINEARLY (TO WITHIN 20%) WITH IMAGINARY INDEX.  
 WAVELENGTH =  $3.8\mu\text{m}$ ; REAL INDEX = 1.5

Geometric Mean Radius $r_g$ ( $\mu\text{m}$ )	Geometric Standard Deviation ( $\sigma_g$ )	$k_{\ell}$
0.1	1.5	1.0
0.1	2.0	1.0
0.1	2.5	0.05
0.25	1.5	1.0
0.25	2.0	0.1
0.25	2.5	0.05
0.5	1.5	0.25
0.5	2.0	0.05
0.5	2.5	0.01
1.0	1.5	0.1
1.0	2.0	0.025
1.0	2.5	0.01

TABLE 5. VALUES OF IMAGINARY INDEX  $k_{\ell}$  BELOW WHICH THE ABSORPTION COEFFICIENT VARIES LINEARLY (WITHIN 20%) WITH IMAGINARY INDEX  $k$ .  
 WAVELENGTH =  $10.6\mu\text{m}$ ; REAL INDEX = 1.8

Geometric Mean Radius $r_g$ ( $\mu\text{m}$ )	Geometric Standard Deviation ( $\sigma_g$ )	$k_{\ell}$
0.1	1.5	1.0
0.1	2.0	1.0
0.1	2.5	0.25
0.1	3.0	0.1
0.25	1.5	1.0
0.25	2.0	0.5
0.25	2.5	0.1
0.25	3.0	0.025
0.5	1.5	1.0
0.5	2.0	0.1
0.5	2.5	0.05
0.5	3.0	0.01
0.75	1.5	1.0
0.75	2.0	0.1
0.75	2.5	0.025
0.75	3.0	0.01
1.0	1.5	0.5
1.0	2.0	0.05
1.0	2.5	0.01
1.0	3.0	0.01
5.0	1.5	0.025
5.0	2.0	0.01
5.0	2.5	0.005

TABLE 6. VALUES OF IMAGINARY INDEX BELOW WHICH THE ABSORPTION COEFFICIENT VARIES LINEARLY (WITHIN 20%) WITH IMAGINARY INDEX  $k$  REAL INDEX = 1.8

Geometric Mean Radius ( $r_g/\lambda$ ) Wavelength	0.01	0.025	0.05	0.1	0.5	1.0
	Values of $k_\ell$					
Geometric Standard Deviation ( $\sigma_g$ )						
1.5	1.0	1.0	1.0	0.5	0.025	0.01
2.0	1.0	0.5	0.1	0.05	0.01	0.005
2.5	0.25	0.1	0.05	0.01	0.005	0.001

TABLE 7. VALUES OF IMAGINARY INDEX  $k_c$  ABOVE WHICH THE ABSORPTION COEFFICIENT IS CONSTANT (TO WITHIN ABOUT 40%) WITH IMAGINARY INDEX. WAVELENGTH =  $3.8\mu\text{m}$ ; REAL INDEX = 1.5

Geometric Mean Radius $r_g$ ( $\mu\text{m}$ )	Geometric Standard Deviation ( $\sigma_g$ )	$k_c$
0.1	1.5	1.0
0.1	2.0	1.0
0.1	2.5	0.5
0.25	1.5	1.0
0.25	2.0	0.5
0.25	2.5	0.25
0.5	1.5	0.5
0.5	2.0	0.25
0.5	2.5	0.1
1.0	1.5	0.25
1.0	2.0	0.1
1.0	2.5	0.05

TABLE 8. VALUES OF IMAGINARY INDEX  $k_c$  ABOVE WHICH THE ABSORPTION COEFFICIENT IS CONSTANT (TO WITHIN 40%) WITH IMAGINARY INDEX WAVELENGTH = 10.6 $\mu$ m; REAL INDEX = 1.8

Geometric Mean Radius $r_g$ ( $\mu$ m)	Geometric Standard Deviation ( $\sigma_g$ )	$k_c$
0.1	1.5	1.0
0.1	2.0	1.0
0.1	2.5	1.0
0.1	3.0	1.0
0.25	1.5	1.0
0.25	2.0	1.0
0.25	2.5	0.5
0.25	3.0	0.25
0.5	1.5	1.0
0.5	2.0	1.0
0.5	2.5	0.25
0.5	3.0	0.25
0.75	1.5	1.0
0.75	2.0	0.5
0.75	2.5	0.25
0.75	3.0	0.1
1.0	1.5	1.0
1.0	2.0	0.25
1.0	2.5	0.1
1.0	3.0	0.1
5.0	1.5	0.1
5.0	2.0	0.05
5.0	2.5	0.025

TABLE 9. VALUES OF IMAGINARY INDEX  $k_c$  ABOVE WHICH THE ABSORPTION COEFFICIENT IS CONSTANT (TO WITHIN 40%) WITH IMAGINARY INDEX REAL INDEX = 1.8

Geometric Mean Radius $r_g$ Wavelength $\lambda$	0.01	0.025	0.05	0.1	0.5	1.0
	Values of $k_c$					
Geometric Standard Deviation $\sigma_g$						
1.5	1.0	1.0	1.0	1.0	0.1	0.05
2.0	1.0	1.0	1.0	0.25	0.05	0.025
2.5	1.0	0.5	0.25	0.1	0.025	0.01

TABLE 10  
 VOLUME ABSORPTION COEFFICIENT AT IMAGINARY INDEX k  
 VOLUME ABSORPTION COEFFICIENT AT IMAGINARY INDEX k = 0.05

Geometric Mean Radius		$r_g/\lambda$	0.01	0.025	0.05	0.1	0.25	0.5	1.0
Wavelength	Imaginary Index k								
$\sigma_g = 1.5$	0.001		0.02	0.02	0.02	0.02	0.03	0.03	0.05
	0.0025		0.05	0.05	0.05	0.05	0.06	0.08	0.12
	0.005		0.10	0.10	0.10	0.11	0.13	0.16	0.23
	0.01		0.20	0.20	0.20	0.21	0.24	0.30	0.39
	0.025		0.50	0.50	0.50	0.51	0.56	0.63	0.73
	0.05		1.00	1.00	1.00	1.00	1.00	1.00	1.00
	0.10		2.00	2.00	1.99	1.90	1.63	1.38	1.18
	0.25		4.98	4.97	4.87	4.18	2.55	1.68	1.22
	0.50		9.84	9.82	9.43	7.01	3.06	1.69	1.17
	1.0		18.21	18.32	17.26	10.63	3.27	1.61	1.09
	2.0*		20.43	21.60	21.94	12.13	2.91	1.36	0.90
	4.0		5.93	7.11	8.87	5.78	1.44	0.70	0.49
6.0		2.16	3.13	4.03	2.74	0.72	0.36	0.26	
8.0		1.17	1.99	2.38	1.56	0.42	0.21	0.15	
$\sigma_g = 2.0$	0.001		0.02	0.02	0.02	0.03	0.04	0.06	0.09
	0.0025		0.05	0.05	0.06	0.06	0.09	0.13	0.19
	0.05		0.10	0.10	0.11	0.13	0.17	0.23	0.34
	0.01		0.20	0.20	0.22	0.25	0.32	0.40	0.54
	0.025		0.50	0.51	0.53	0.57	0.65	0.73	0.83
	0.05		1.00	1.00	1.00	1.00	1.00	1.00	1.00
	0.10		2.00	1.96	1.82	1.63	1.37	1.20	1.08
	0.25		4.07	4.62	3.77	2.65	1.70	1.29	1.09
	0.50		9.79	8.50	5.72	3.41	1.80	1.27	1.05
	1.0		18.22	14.54	8.24	4.06	1.77	1.18	0.96
	2.0*		21.67	17.62	9.13	3.95	1.52	0.98	0.78
	4.0		7.26	7.39	4.24	1.94	0.78	0.53	0.44
6.0		3.14	3.41	2.02	0.95	0.40	0.28	0.24	
8.0		1.92	2.00	1.16	0.55	0.23	0.16	0.14	
$\sigma_g = 2.5$	0.001		0.02	0.02	0.03	0.04	0.06	0.10	0.16
	0.0025		0.05	0.06	0.07	0.09	0.14	0.21	0.33
	0.005		0.10	0.12	0.14	0.18	0.25	0.36	0.51
	0.01		0.21	0.23	0.27	0.32	0.43	0.55	0.71
	0.025		0.51	0.55	0.59	0.65	0.75	0.83	0.92
	0.05		1.00	1.00	1.00	1.00	1.00	1.00	1.00
	0.10		1.92	1.72	1.55	1.39	1.20	1.09	1.03
	0.25		4.37	3.15	2.36	1.80	1.32	1.11	1.02
	0.50		7.76	4.59	2.96	2.00	1.31	1.08	0.99
	1.0		12.87	6.28	3.50	2.09	1.24	0.99	0.90
	2.0*		15.21	6.76	3.43	1.87	1.03	1.81	0.71
	4.0		6.35	3.03	1.67	0.95	0.55	0.45	0.41
6.0		2.93	1.50	0.32	0.48	0.29	0.24	—	
8.0		1.72	0.87	0.48	0.28	0.17	0.15	—	

\*Applicable Only to Wavelengths  $\gtrsim 2\mu\text{m}$  For  $k \lesssim 2.0$ . Real Index = 1.6

TABLE 11. VALUES OF THE RATIO OF ABSORPTION COEFFICIENTS  
 $\sigma_A(n)/\sigma_A(n = 1.4)$  FOR REALISTIC SIZE DISTRIBUTIONS  
 IMAGINARY INDEX  $k = 0.025$ ; WAVELENGTH  $\lambda = 3.8\mu\text{m}$

$n/\sigma_g$	$\sigma_A(n)/\sigma_A(n = 1.4)$											
	$r_g = 0.1\mu\text{m}$			$r_g = 0.25\mu\text{m}$			$r_g = 0.5\mu\text{m}$			$r_g = 1.0\mu\text{m}$		
	1.5	2.0	2.5	1.5	2.0	2.5	1.5	2.0	2.5	1.5	2.0	2.5
1.4	1.0	1.0	1.0	1.0	1.0	1.0	1.0	1.0	1.0	1.0	1.0	1.0
1.7	0.82	0.97	1.25	0.93	1.26	1.23	1.23	1.30	1.15	1.36	1.20	1.06
2.0	0.66	1.03	1.48	0.89	1.60	1.44	1.60	1.56	1.22	1.74	1.35	1.07
2.25	0.55	1.13	1.72	0.96	1.92	1.55	2.05	1.73	1.25	1.98	1.37	1.05
2.5	0.46	1.34	1.94	1.17	2.22	1.63	2.54	1.84	1.26	2.13	1.37	1.03
3.0	0.33	2.03	2.33	1.85	2.75	1.71	3.52	1.96	1.24	2.16	1.33	0.98

TABLE 12. VALUES OF THE RATIO OF ABSORPTION COEFFICIENTS  
 $\sigma_A(n)/\sigma_A(n = 1.2)$  FOR REALISTIC SIZE DISTRIBUTIONS  
 IMAGINARY INDEX  $k = 0.025$ ; WAVELENGTH  $\lambda = 10.6\mu\text{m}$

$n/\sigma_g$	$\sigma_A(n)/\sigma_A(n = 1.2)$											
	$r_g = 0.25\mu\text{m}$			$r_g = 0.5\mu\text{m}$			$r_g = 0.75\mu\text{m}$			$r_g = 1.0\mu\text{m}$		
	1.5	2.0	2.5	1.5	2.0	2.5	1.5	2.0	2.5	1.5	2.0	2.5
1.2	1.0	1.0	1.0	1.0	1.0	1.0	1.0	1.0	1.0	1.0	1.0	1.0
1.6	0.77	0.90	1.09	0.84	1.06	1.15	0.93	1.13	1.16	1.02	1.17	1.15
2.0	0.57	0.83	1.19	0.68	1.15	1.26	0.88	1.28	1.25	1.09	1.32	1.22
2.5	0.39	0.84	1.32	0.55	1.33	1.35	0.97	1.46	1.29	1.34	1.46	1.22
3.0	0.28	0.98	1.44	0.54	1.53	1.39	1.23	1.59	1.28	1.70	1.52	1.19
4.5	0.15	1.64	1.62	1.37	1.87	1.32	2.37	1.64	1.13	2.38	1.42	1.02
6.5	0.32	2.10	1.50	2.69	1.75	1.09	2.53	1.37	0.91	1.97	1.14	0.78

TABLE 13. VOLUME ABSORPTION COEFFICIENT AT REAL INDEX n  
VOLUME ABSORPTION COEFFICIENT AT REAL INDEX n = 1.33

Geometric Mean Radius Wavelength Real Index n	$r_g/\lambda$	0.01	0.025	0.05	0.1	0.25	0.5	1.0
$\sigma_g = 1.5$	1.33	1.0	1.0	1.0	1.0	1.0	1.0	1.0
	1.5	0.89	0.90	0.93	1.04	1.17	1.16	1.06
	1.7	0.76	0.78	0.85	1.11	1.41	1.29	1.06
	1.9	0.65	0.64	0.77	1.23	1.64	1.35	1.04
	2.2*	0.51	0.54	0.68	1.55	1.92	1.34	0.99
	2.5	0.40	0.43	0.62	2.02	2.07	1.30	0.96
	3.5	0.19	0.24	1.46	3.95	1.96	1.15	0.84
	5.0	0.08	0.17	5.06	5.03	1.67	0.99	0.71
6.5	0.05	1.88	8.41	4.55	1.50	0.86	0.61	
$\sigma_g = 2.0$	1.33	1.0	1.0	1.0	1.0	1.0	1.0	1.0
	1.5	0.90	0.97	1.08	1.15	1.13	1.06	1.0
	1.7	0.79	0.94	1.20	1.34	1.21	1.08	0.98
	1.9	0.68	0.95	1.36	1.53	1.30	1.08	0.95
	2.2*	0.55	1.03	1.67	1.77	1.33	1.04	0.91
	2.5	0.45	1.18	2.02	1.95	1.32	1.01	0.88
	3.5	0.27	2.41	3.01	3.30	1.30	0.89	0.77
	5.0	1.33	4.49	3.74	2.10	1.02	0.75	0.64
6.5	2.92	5.89	4.81	1.90	0.89	0.64	0.55	
$\sigma_g = 2.5$	1.33	1.0	1.0	1.0	1.0	1.0	1.0	1.0
	1.5	0.99	1.11	1.14	1.12	1.05	1.01	0.98
	1.7	1.00	1.26	1.30	1.22	1.08	1.00	0.95
	1.9	1.03	1.42	1.43	1.28	1.08	0.97	0.92
	2.2*	1.18	1.67	1.59	1.34	1.06	0.93	0.88
	2.5	1.39	1.690	1.70	1.36	1.02	0.89	0.85
	3.5	2.43	2.50	1.86	1.31	0.90	0.79	0.74
	5.0	3.89	2.89	1.81	1.16	0.77	0.66	0.62
6.5	4.93	2.94	1.67	0.99	0.66	0.56	-	

\* Applicable Only to Wavelengths  $> 2\mu\text{m}$  For  $n > 2.2$  Imaginary Index = 0.05

TABLE 14. THE RANGE OF IMAGINARY k, FOR A RANGE OF REAL INDEX n USING A RANGE OF ISOABSORPTION COEFFICIENTS FOR  $10.6\mu\text{m}$  WAVELENGTH

Imaginary Index k	Real Index n	Isoabsorption Value ( $\text{km}^{-1}$ )	Geometric Standard Deviation
$r_g = 0.1\mu\text{m}$			
0.004 - 0.02	0.1 - 5.0	$1.6 \times 10^{-4}$	2.0
0.004 - 0.06	1.0 - 3.0	$1.6 \times 10^{-4}$	2.0
0.008 - 0.2	0.1 - 7.0	$1.6 \times 10^{-3}$	2.0
0.04 - 0.16	1.0 - 3.0	$1.6 \times 10^{-3}$	2.0
0.2 - 1.0	0.1 - 4.0	$8 \times 10^{-3}$	2.0
0.2 - 0.7	1.0 - 3.0	$8 \times 10^{-3}$	2.0
0.3 - 1.5	0.1 - 3.25	$1.2 \times 10^{-2}$	2.0
0.3 - 1.0	1.0 - 3.0	$1.2 \times 10^{-2}$	2.0
$r_g = 1.0\mu\text{m}$			
0.04 - 0.001	0.1 - 3.5	$2.4 \times 10^{-4}$	1.5
0.0014 - 0.006	1.0 - 3.0	$2.4 \times 10^{-4}$	1.5
0.155 - 0.002	0.1 - 4.5	$1 \times 10^{-3}$	1.5
0.006 - 0.022	1.0 - 3.0	$1 \times 10^{-3}$	1.5
0.004 - 0.4	0.1 - 8.0	$2.4 \times 10^{-3}$	1.5
0.015 - 0.06	1.0 - 3.0	$2.4 \times 10^{-3}$	1.5
0.02 - 0.8	0.1 - 5.5	$6 \times 10^{-3}$	1.5
0.005 - 1.5	1.0 - 3.0	$6 \times 10^{-3}$	1.5
0.1 - 2.0	0.1 - 8.0	$2 \times 10^{-2}$	1.5
0.4 - 0.6	1.0 - 3.0	$2 \times 10^{-2}$	1.5
$r_g = 10.0\mu\text{m}$			
0.002 - 0.2	0.1 - 6.5	$2 \times 10^{-4}$	1.5
0.002 - 0.005	1.0 - 3.0	$2 \times 10^{-4}$	1.5
0.03 - 0.8	0.1 - 8.0	$1.6 \times 10^{-3}$	1.5
0.03 - 0.09	1.0 - 3.0	$1.6 \times 10^{-3}$	1.5
0.09 - 0.6	0.1 - 8.0	$2.25 \times 10^{-3}$	1.5
0.09 - 0.6	1.0 - 3.0	$2.25 \times 10^{-3}$	1.5

TABLE 15. THE RANGE OF IMAGINARY INDEX  $k$  FOR RANGES OF REAL INDEX  $n$   
 USING A SELECTION OF ISOABSORPTION VALUES FOR 3.8 $\mu$ m WAVELENGTH

Imaginary Index $k$	Real Index $n$	Absorption Coefficient ( $\text{km}^{-1}$ ) (normalized to mass = 100 $\mu\text{g m}^{-3}$ )	Geometric Mean Radius, $r_g$ ( $\mu\text{m}$ )	Geometric Standard Deviation $\cdot\sigma_g$
0.005 - 0.015	1.2 - 3.0	$5 \times 10^{-4}$	0.1	1.5
0.005 - 0.008	1.2 - 2.0	$5 \times 10^{-4}$	0.1	1.5
0.014 - 0.05	1.2 - 3.0	$1.6 \times 10^{-3}$	0.1	1.5
0.014 - 0.025	1.2 - 2.0	$1.6 \times 10^{-3}$	0.1	1.5
0.05 - 0.15	1.2 - 3.0	$5.0 \times 10^{-3}$	0.1	1.5
0.05 - 0.065	1.2 - 2.0	$5.0 \times 10^{-3}$	0.1	1.5
0.085 - 0.3	1.2 - 3.0	$1.0 \times 10^{-2}$	0.1	1.5
0.085 - 0.15	1.2 - 2.0	$1.0 \times 10^{-2}$	0.1	1.5
0.014 - 0.01	1.2 - 3.0	$1.6 \times 10^{-3}$	0.1	2.0
0.014 - 0.013	1.2 - 2.0	$1.6 \times 10^{-3}$	0.1	2.0
0.05 - 0.025	1.2 - 3.0	$6.0 \times 10^{-3}$	0.1	2.0
0.05 - 0.05	1.2 - 2.0	$6.0 \times 10^{-3}$	0.1	2.0
0.085 - 0.05	1.2 - 3.0	$1.0 \times 10^{-2}$	0.1	2.0
0.085 - 0.1	1.2 - 2.0	$1.0 \times 10^{-2}$	0.1	2.0
0.01 - 0.003	1.2 - 3.0	$1.6 \times 10^{-3}$	0.5	1.5
0.01 - 0.007	1.2 - 2.0	$1.6 \times 10^{-3}$	0.5	1.5
0.05 - 0.01	1.2 - 3.0	$6.0 \times 10^{-3}$	0.5	1.5
0.05 - 0.025	1.2 - 2.0	$6.0 \times 10^{-3}$	0.5	1.5
0.085 - 0.02	1.2 - 3.0	$1.0 \times 10^{-2}$	0.5	1.5
0.085 - 0.05	1.2 - 2.0	$1.0 \times 10^{-2}$	0.5	1.5
0.2 - 0.05	1.2 - 3.0	$2.0 \times 10^{-2}$	0.5	1.5
0.2 - 0.1	1.2 - 2.0	$2.0 \times 10^{-2}$	0.5	1.5
0.01 - 0.005	1.2 - 3.0	$1.6 \times 10^{-3}$	0.5	2.25
0.01 - 0.007	1.2 - 2.0	$1.6 \times 10^{-3}$	0.5	2.25
0.065 - 0.025	1.2 - 3.0	$6 \times 10^{-3}$	0.5	2.25
0.065 - 0.035	1.2 - 2.0	$6 \times 10^{-3}$	0.5	2.25
0.2 - 0.085	1.2 - 3.0	$1.0 \times 10^{-2}$	0.5	2.25
0.2 - 0.085	1.2 - 2.0	$1.0 \times 10^{-2}$	0.5	2.25
0.01 - 0.0025	1.2 - 3.0	$1.6 \times 10^{-3}$	1.0	1.5
0.01 - 0.005	1.2 - 2.0	$1.6 \times 10^{-3}$	1.0	1.5
0.05 - 0.014	1.2 - 3.0	$6.0 \times 10^{-3}$	1.0	1.5
0.05 - 0.02	1.2 - 2.0	$6.0 \times 10^{-3}$	1.0	1.5
0.085 - 0.025	1.2 - 3.0	$1.0 \times 10^{-2}$	1.0	1.5
0.085 - 0.035	1.2 - 2.0	$1.0 \times 10^{-2}$	1.0	1.5
0.35 - 0.1	1.2 - 3.0	$2.0 \times 10^{-2}$	1.0	1.5
0.35 - 0.1	1.2 - 2.0	$2.0 \times 10^{-2}$	1.0	1.5
0.01 - 0.005	1.2 - 3.0	$1.6 \times 10^{-3}$	1.0	2.0
0.01 - 0.006	1.2 - 2.0	$1.6 \times 10^{-3}$	1.0	2.0
0.065 - 0.035	1.2 - 3.0	$6.0 \times 10^{-3}$	1.0	2.0
0.065 - 0.035	1.2 - 2.0	$6.0 \times 10^{-3}$	1.0	2.0
0.35 - 0.1	1.2 - 3.0	$1.0 \times 10^{-2}$	1.0	2.0
0.35 - 0.1	1.2 - 2.0	$1.0 \times 10^{-2}$	1.0	2.0

TABLE 16. A COMPARISON OF THE VARIATION, IN IMAGINARY INDEX  $k$  WITH CHANGES IN REAL INDEX FOR A SELECTION OF PARTICLE SIZE DISTRIBUTIONS USING TWO ISOABSORPTION VALUES: WAVELENGTH =  $10.6\mu\text{m}$

Variation in Imaginary Index $k$	ISOABSORPTION VALUE = $2 \times 10^{-4} \text{ km}^{-1}$		
	Range of Real Index $n$	Geometric Mean Radius ( $\mu$ )	Geometric Standard Deviation
0.005 - 0.02	0.1 - 3.25	0.1	2.0
0.001 - 0.03	0.1 - 3.25	1.0	2.5
0.001 - 0.2	0.1 - 3.25	10.0	1.5
ISOABSORPTION VALUE = $1.6 \times 10^{-3} \text{ km}^{-1}$			
0.008 - 0.2	0.1 - 7.0	0.1	2.0
0.002 - 0.25	0.1 - 8.0	1.0	1.5
0.03 - 0.8	0.1 - 8.0	10.0	1.5
0.04 - 0.2	1.0 - 3.0	0.1	2.0
0.01 - 0.04	1.0 - 3.0	1.0	1.5
0.03 - 0.09	1.0 - 3.0	10.0	1.5

TABLE 17. THE RATIO OF ABSORPTION TO EXTINCTION FOR A WIDE RANGE OF REALISTIC PARTICLE SIZE DISTRIBUTIONS AT WAVELENGTHS 0.694, 3.8, AND  $10.6\mu\text{m}$

Geometric Mean Radius ( $\mu\text{m}$ )	Geometric Standard Deviation	Wavelength ( $\mu\text{m}$ )	Imaginary Index							
			0.005	0.01	0.05	0.1	0.25	0.5	1.0	
PERCENTAGE OF ABSORPTION/EXTINCTION										
0.1	1.5	0.694	2.6	5.1	21.5	35.4	56.0			
		3.8		76.1	93.9	96.7	98.8			
		10.6			99.2	99.6	99.8	99.8	99.9	
0.1	2.0	0.694	3.0	5.8	21.9	33.9	50.2			
		3.8		16.7	50.6	67.3	82.1			
		10.6			83.8	91.0	96.0	97.0	97.2	
0.1	2.5	0.694	5.9	10.5	30.0	39.8	49.8			
		3.8		6.0	24.7	40.0	61.0			
		10.6			26.2	42.1	64.8	77.0	79.8	
0.25	1.5	0.694	2.7	5.2	20.5	32.2	48.1			
		3.8		20.7	57.0	71.8	84.6			
		10.6			89.0	94.2	97.4	98.2	98.4	
0.25	2.0	0.694	6.2	11.1	31.8	41.5	50.0			
		3.8		6.0	24.8	40.0	61.1			
		10.6			32.6	49.5	70.4	80.1	82.1	
0.25	2.5	0.694	11.9	18.9	39.5	45.5	48.9			
		3.8		7.0	25.1	37.6	53.7			
		10.6			19.0	31.3	51.1	62.8	66.4	
1.0	1.5	0.694	12.2	20.4	44.5	49.1	50.0			
		3.8		4.8	19.9	32.9	51.7			
		10.6			21.5	35.6	55.8	68.6	71.0	
1.0	2.0	0.694	18.9	28.4	45.8	47.6	47.5			
		3.8		8.3	27.3	38.5	50.7			
		10.6			18.7	30.1	47.5	57.6	59.5	
1.0	2.5	0.694	27.6	35.8	45.8	46.4	46.0			
		3.8		15.4	36.0	43.9	50.1			
		10.6			26.1	36.0	48.2	53.4	52.7	
5.0	1.5	0.694	32.2	40.5	45.6	45.7	45.1			
		3.8		19.4	44.3	49.8	50.6			
		10.6			28.5	39.6	52.1	52.2	49.4	
5.0	2.0	0.694	38.2	43.3	45.3	45.3	44.7			
		3.8		27.5	46.3	48.6	48.5			
		10.6			36.9	44.9	49.4	49.3	46.1	
5.0	2.5	3.8		35.4	46.5	47.3	47.0			
		10.6			41.8	46.0	47.7	45.8	43.2	

Real Index = 1.6 For  $\lambda = 0.69\mu\text{m}$   
 = 1.5 For  $\lambda = 3.8\mu\text{m}$   
 = 1.8 For  $\lambda = 10.6\mu\text{m}$

TABLE 18. VALUES OF LOGNORMAL PARTICLE SIZE DISTRIBUTION PARAMETERS (GEOMETRIC RADIUS  $r_g$  AND GEOMETRIC STANDARD DEVIATION  $\sigma_g$ ) AND MASS LOADINGS FOR BIMODAL DISTRIBUTIONS REPRESENTATIVE OF DESERT AEROSOLS

(a) Light Aerosol Loading

$r_g$ ( $\mu\text{m}$ )	$\sigma_g$	Mass ( $\mu\text{g m}^{-3}$ )
0.05	2.0	20
0.5	2.0	40

(b) Heavy Aerosol Loading

$r_g$ ( $\mu\text{m}$ )	$\sigma_g$	Mass ( $\mu\text{g m}^{-3}$ )
0.5	2.25	$5 \times 10^3$
15.0	1.6	$1 \times 10^4$

TABLE 19. VALUES OF COMPLEX REFRACTIVE INDEXES FOR A BIMODAL PARTICLE SIZE DISTRIBUTION CHARACTERISTIC OF "LIGHT" AND "HEAVY" DESERT AEROSOL LOADINGS. TYPICAL VALUES OF COMPLEX REFRACTIVE INDEX ARE PRESENTED, AS WELL AS VALUES WHICH RESULT IN MINIMUM AND MAXIMUM AEROSOL EXTINCTION.

Wavelength ( $\mu\text{m}$ )		Light Aerosol Loading				Heavy Aerosol Loading			
		Small Particle Mode		Large Particle Mode		Small Particle Mode		Large Particle Mode	
		Real Index of Refraction	Imaginary Index of Refraction	Real Index of Refraction	Imaginary Index of Refraction	Real Index of Refraction	Imaginary Index of Refraction	Real Index of Refraction	Imaginary Index of Refraction
0.55	Minimum	1.52	0.01	1.52	0.0001	1.5	0.0001	1.5	0.0001
	Typical	1.54	0.015	1.54	0.003	1.5	0.003	1.5	0.0001
	Maximum	1.6	0.03	1.6	0.005	1.6	0.005	1.6	0.005
1.06	Minimum	1.5	0.01	1.5	0.0001	1.50	0.001	1.5	0.0001
	Typical	1.54	0.015	1.5	0.001	1.52	0.001	1.5	0.0001
	Maximum	1.6	0.06	1.6	0.005	1.60	0.005	1.6	0.005
3.8	Minimum	1.56	0.02	1.25	0.001	1.25	0.001	1.25	0.001
	Typical	1.6	0.2	1.5	0.02	1.5	0.02	1.5	0.01
	Maximum	1.8	1.0	1.8	0.05	1.8	0.05	1.8	0.05
9.3	Minimum	4.55	3.65	1.26	0.05	1.26	0.05	3.43	7.51
	Typical	2.5	1.5	2.2	0.5	2.2	0.5	2.2	0.5
	Maximum	2.23	1.07	0.86	1.44	0.86	1.44	0.86	1.44
10.6	Minimum	1.00	0.06	1.19	0.07	1.19	0.07	2.18	0.02
	Typical	2.2	1.25	1.7	0.2	1.7	0.2	1.7	0.2
	Maximum	2.04	1.28	2.18	0.02	2.18	0.02	1.19	0.07

TABLE 20. VALUES OF EXTINCTION COEFFICIENT ( $\text{km}^{-1}$ ) CORRESPONDING TO THE COMPLEX REFRACTIVE INDEX VALUES GIVEN IN TABLE 19. THE CALCULATIONS ARE FOR A BIMODAL PARTICLE SIZE DISTRIBUTION CHARACTERISTIC OF "LIGHT" AND "HEAVY" DESERT AEROSOL LOADINGS GIVEN IN TABLE 18.

Wavelength ( $\mu\text{m}$ )	Light Aerosol Loading		Heavy Aerosol Loading	
	Small Particle Mode (mass = $20\mu\text{g m}^{-3}$ )	Large Particle Mode (mass = $60\mu\text{g m}^{-3}$ )	Small Particle Mode (mass = $5 \times 10^3\mu\text{g m}^{-3}$ )	Large Particle Mode (mass = $10^4\mu\text{g m}^{-3}$ )
	Extinction Coefficient ( $\text{km}^{-1}$ )	Extinction Coefficient ( $\text{km}^{-1}$ )	Extinction Coefficient ( $\text{km}^{-1}$ )	Extinction Coefficient ( $\text{km}^{-1}$ )
0.55	0.0482	0.0164	1.27	0.183
	0.0506	0.0163	1.27	0.183
	0.0566	0.0162	1.26	0.183
1.06	0.0135	0.0189	1.42	0.23
	0.0158	0.0189	1.42	0.14
	0.0212	0.0186	1.40	0.23
3.8	0.0006	0.0064	0.80	0.24
	0.0038	0.0137	1.30	0.18
	0.015	0.018	1.52	0.28
9.3	0.0018	0.0019	0.32	0.22
	0.0038	0.0122	1.22	0.25
	0.0038	0.020	1.67	0.26
10.6	0.0003	0.0015	0.22	0.26
	0.0038	0.0064	0.81	0.26
	0.0043	0.0095	1.12	0.26

TABLE 21. VALUES OF COMPLEX REFRACTIVE INDEXES FOR A BIMODAL PARTICLE SIZE DISTRIBUTION CHARACTERISTIC OF "LIGHT" AND "HEAVY" DESERT AEROSOL LOADINGS. TYPICAL VALUES OF COMPLEX REFRACTIVE INDEX ARE PRESENTED, AS WELL AS VALUES WHICH RESULT IN MINIMUM AND MAXIMUM AEROSOL ABSORPTION.

Wavelength ( $\mu\text{m}$ )		Light Aerosol Loading				Heavy Aerosol Loading			
		Small Particle Mode		Large Particle Mode		Small Particle Mode		Large Particle Mode	
		Real Index of Refraction	Imaginary Index of Refraction	Real Index of Refraction	Imaginary Index of Refraction	Real Index of Refraction	Imaginary Index of Refraction	Real Index of Refraction	Imaginary Index of Refraction
0.55	Minimum	1.52	0.01	1.52	0.0001	1.5	0.0001	1.5	0.0001
	Typical	1.54	0.015	1.54	0.003	1.5	0.003	1.5	0.003
	Maximum	1.6	0.03	1.6	0.005	1.6	0.005	1.6	0.005
1.06	Minimum	1.5	0.01	1.5	0.0001	1.50	0.0001	1.5	0.0001
	Typical	1.54	0.015	1.5	0.001	1.52	0.001	1.5	0.001
	Maximum	1.6	0.06	1.6	0.005	1.60	0.005	1.6	0.005
3.8	Minimum	1.56	0.02	1.25	0.001	1.25	0.001	1.25	0.001
	Typical	1.6	0.2	1.5	0.02	1.5	0.02	1.5	0.01
	Maximum	1.8	1.0	1.47	0.13	1.8	0.05	1.8	0.05
9.3	Minimum	4.55	3.65	1.26	0.05	1.26	0.05	3.43	7.51
	Typical	2.5	1.5	2.2	0.5	2.2	0.5	2.2	0.5
	Maximum	2.23	1.07	0.86	1.44	0.86	1.44	1.72	0.162
10.6	Minimum	1.99	0.06	1.19	0.07	1.7	0.015	1.7	0.015
	Typical	2.2	1.25	1.7	0.2	1.7	0.2	1.7	0.2
	Maximum	2.04	1.28	1.7	0.06	1.7	0.6	1.16	0.17

TABLE 22. VALUES OF ABSORPTION COEFFICIENT ( $\text{km}^{-1}$ ) CORRESPONDING TO THE COMPLEX REFRACTIVE INDEX VALUES GIVEN IN TABLE 21. THE CALCULATIONS ARE FOR A BIMODAL PARTICLE SIZE DISTRIBUTION CHARACTERISTIC OF "LIGHT" AND "HEAVY" DESERT AEROSOL LOADINGS GIVEN IN TABLE 18.

Wavelength ( $\mu\text{m}$ )	Light Aerosol Loading		Heavy Aerosol Loading	
	Small Particle Mode (mass = $20\mu\text{g m}^{-3}$ )	Large Particle Mode (mass = $60\mu\text{g m}^{-3}$ )	Small Particle Mode (mass = $5 \times 10^3\mu\text{g m}^{-3}$ )	Large Particle Mode (mass = $10^4\mu\text{g m}^{-3}$ )
	Absorption Coefficient ( $\text{km}^{-1}$ )	Absorption Coefficient ( $\text{km}^{-1}$ )	Absorption Coefficient ( $\text{km}^{-1}$ )	Absorption Coefficient ( $\text{km}^{-1}$ )
0.55	0.0026	0.0006	0.007	0.004
	0.0038	0.0013	0.155	0.004
	0.0073	0.0023	0.225	0.080
1.06	0.00104	0.00003	0.004	0.006
	0.0016	0.0003	0.037	0.006
	0.006	0.0015	0.154	0.092
3.8	0.0004	0.0006	0.008	0.016
	0.0036	0.0015	0.173	0.042
	0.014	0.0055	0.38	0.12
9.3	0.0017	0.0010	0.11	0.03
	0.0037	0.0068	0.65	0.11
	0.0038	0.0134	0.99	0.12
10.6	0.0003	0.0012	0.05	0.07
	0.0038	0.0033	0.38	0.12
	0.0049	0.0067	0.64	0.13

## REFERENCES

1. Hoidale, G. B., and A. J. Blanco, 1969, "Infrared Absorption Spectra of Atmospheric Dust over an Interior Desert Basin," Pure and Appl. Geophys., 74:157-164.
2. Blanco, A. J., and R. G. McIntyre, 1972, "An Infra-Red Spectroscopic View of Atmospheric Particulates over El Paso, TX," Atmos. Environ., 6:557-562.
3. Patterson, E. M., and D. A. Gillette, 1977, "Commonalities in Measured Size Distributions for Aerosols having a Soil-Derived Component," J. Geophys. Res., 82:2074-2082.
4. Lindberg, J. D., and J. B. Gillespie, 1977, "Relationship Between Particle Size and Imaginary Refractive Index in Atmospheric Dust," Appl. Opt., 16:2628-2630.
5. Toon, O. B., J. B. Pollack, and C. Sagan, 1977, "Physical Properties of the Particles Composing the Martian Dust Storm of 1971-1972," Icarus, 30:663-696.
6. Toon, O. B., J. B. Pollack, and B. N. Khare, 1976, "Optical Constants of Several Atmospheric Aerosol Species, Ammonium Sulphate, Aluminum Oxide and Sodium Chloride," J. Geophys. Res., 81:5733-5748.
7. Cartwright, J., G. Nagelshmidt, and J. W. Skidmore, 1956, "The Study of Air Pollution with an Electron Microscope," Quart. J. Roy. Meteorol. Soc., 82:82-86.
8. Meszaros, A., and K. Vissy, 1974, "Concentration, Size Distribution and Chemical Nature of Atmospheric Aerosol Particle in Remote Oceanic Areas," Aerosol Science, 5:101-109.
9. Durham, J. L., W. E. Wilson, T. G. Ellestad, K. Willeke, and K. T. Whitby, 1975, "Comparison of Volume and Mass Distributions for Denver Aerosols," Atmos. Environ., 9:717-722.
10. Charlson, R. J., A. H. Vanderpol, D. S. Covert, A. P. Waggoner, and N. C. Ahlquist, 1974, "Sulphuric Acid-Ammonium Sulphate Aerosol: Optical Detection in St. Louis Region," Science, 184:156-158.
11. Patterson, R. K., and J. Wagman, 1977, "Mass and Composition of an Urban Aerosol as a Function of Particle Size for Several Visibility Levels," Aerosol Science, 8:269-279.
12. Bergstrom, R. W., 1973, "Extinction and Absorption Coefficients of the Atmospheric Aerosol as a Function of Particle Size," Beitr. Phys. Atmos., 46:223-234.

13. Hänel, G., and K. Bullrich, 1970, "Calculations of the Spectral Extinction Coefficients of Atmospheric Aerosol Particles with Different Complex Refractive Indices," Beitr. Phys. Atmos., 43:202-207.
14. Willeke, K., and J. E. Brockmann, 1977, "Extinction Coefficients for Multimodal Atmospheric Particle Size Distributions," Atmos. Environ., 11:995-999.
15. Patterson, E. M., 1977, "Atmospheric Extinction Between 0.55 $\mu$ m and 10.6 $\mu$ m due to Soil Derived Aerosols," Appl. Opt., 16:2414-2418.
16. Dave, J. V., 1968, Report NO-320-3237, IBM Scientific Center, Palo Alto, California.
17. van de Hulst, H. C., 1957, Light Scattering by Small Particles, New York: Wiley.
18. Deirmendjian, D., 1969, Electromagnetic Scattering on Spherical Polydispersions, New York: Elsevier.
19. Kerker, M., 1969, The Scattering of Light and Other Electromagnetic Radiation, New York: Academic Press.
20. Whitby, K. T., R. B. Husar, and B. Y. H. Liu, 1972, "The Aerosol Size Distribution of Los Angeles Smog," J. Coll. Inter. Sci., 39:177-204.
21. Davies, C. N., 1974, "Size Distributions of Atmospheric Particles," Aerosol Science, 5:293-300.
22. Dalzell, W. H., and A. F. Sarofim, 1969, "Optical Constants of Soot and Their Application to Heat Flux Calculations," J. Heat Transfer, 91:100-104.
23. Foster, P. J., and C. R. Howarth, 1968, "Optical Constants of Carbons and Coals in the Infrared," Carbon, 6:719-729.
24. Spitzer, W. G., and D. A. Kleinman, 1961, "Infrared Lattice Bands of Quartz," Phys. Rev., 121:1324-1335.
25. Volz, F. E., 1972, "Infrared Refractive Index of Atmospheric Aerosol Substances," Appl. Opt., 11:755-759.
26. Volz, F. E., 1973, "Infrared Optical Constants of Ammonium Sulphate, Sahara Dust, Volcanic Pumice and Fly Ash," Appl. Opt., 12:564-568.
27. Fischer, K., 1970, "Bestimmung der Absorption von sichtbarer Strahlung durch Aerosolpartikeln," Beitr. Phys. Atmos., 43:244-254.
28. Schleusener, S. A., J. D. Lindberg, K. O. White, and R. L. Johnson, 1976, "Spectrophone Measurements of Infrared Laser Energy Absorption by Atmospheric Dust," Appl. Opt., 15:2546-2550.

29. Bergstrom, R. W., 1973, "Comments on the Estimation of Aerosol Absorption Coefficients in the Atmosphere," Beitr. Phys. Atmos., 46:198-202.
30. Waggoner, A. P., M. B. Baker, and R. J. Charlson, 1973, "Optical Absorption by Atmospheric Aerosols," Appl. Opt., 12:896.
31. Jennings, S. G., 1977, "Mie Theory Sensitivity Studies - The Effects of Aerosol Complex Refractive Index and Size Distribution Variations on Extinction and Absorption Coefficients. Part I: Tabulated Computational Results," Data Report ECOM-DR-77-5, Atmospheric Sciences Laboratory, US Army Electronics Command, White Sands Missile Range, NM. AD A049031
32. Jennings, S. G., and J. B. Gillespie, 1978, "Mie Theory Sensitivity Studies-The Effects of Aerosol Complex Refractive Index and Size Distribution Variations on Extinction and Absorption Coefficients. Part II: Analysis of the Computational Results," ASL-TR-0003, Atmospheric Sciences Laboratory, US Army Electronics R&D Command, White Sands Missile Range, NM.
33. Sverdrup, G. M., K. T. Whitby, and W. E. Clark, 1975, "Characterization of California Aerosols - II: Aerosol Size Distribution Measurements in the Mojave Desert," Atmos. Environ., 9:483-494.
34. Junge, C. E., and R. Jaenicke, 1971, "New Results in Background Aerosols Studies From the Atlantic Expedition of the R. V. Meteor, Spring 1969," Aerosol Science, 2:305-314.
35. De Luisi, J. J., P. M. Furukana, D. A. Gillette, B. G. Schuster, R. T. Charlson, W. M. Porch, R. W. Fegley, B. M. Herman, R. A. Rabinoff, J. T. Twitty, and J. A. Weinman, 1976, "Results of a Comprehensive Atmospheric Aerosol-Radiation Experiment in the Southwestern United States, Part I: Size Distribution, Extinction Optical Depth and Vertical Profiles of Aerosols Suspended in the Atmosphere," J. Appl. Meteorol., 15:441-454.
36. Gillette D. A., and T. R. Walker, 1977, "Characteristics of Airborne Particles Produced by Wind Erosion of Sandy Soil, High Plains of West Texas," Soil Science, 123:97-110.
37. Fischer, K., 1973, "Mass Absorption Coefficients of Natural Aerosol Particles in the 0.4 $\mu$ m - 2.4 $\mu$ m Wavelength Interval," Beitr. Phys. Atmos., 46:89-100.
38. Fischer, K. 1975, "Mass Absorption Indices of Various Types of Natural Aerosol Particles in the Infrared," Appl. Opt., 14:2851-2856.
39. Lindberg, J. D., and L. S. Laude, 1974, "Measurement of the Absorption Coefficient of Atmospheric Dust," Appl. Opt., 13:1923-1927.
40. Hänel, G., 1968, "The Real Part of the Mean Complex Refractive Index and the Mean Density of Samples of Atmospheric Aerosol Particles," Tellus, 20:371-379.

41. Querry, M. R., G. Osborne, K. Lies, R. Jurdan, and R. M. Coveney, 1977, "Complex Refractive Index of Limestone in the Visible and Infrared," Appl. Opt. (in press)
42. Downing, H. D., L. W. Pinkley, P. P. Sethna, and D. Williams, 1977, "Optical Constants of Ammonium Sulphate in the Infrared," J. Opt. Soc. Am., 67:186-190.
43. Grams, G. W., I. H. Blifford, D. A. Gillette, and P. B. Russell, 1974, "Complex Index of Refraction of Airborne Soil Particles," J. Appl. Meteorol., 13:459-471.
44. Gillespie, J. B., S. G. Jennings, and J. D. Lindberg, 1978, "Use of an Average Complex Refractive Index in Atmospheric Propagation Calculations," Appl. Opt., 17:989-991.
45. Chýlek, Petr., 1977, "Extinction Cross Sections of Arbitrarily Shaped Randomly Oriented Nonspherical Particles," J. Opt. Soc. Am., 67:1348-1350.
46. Pinnick, R. G., D. E. Carroll, and D. J. Hoffmann, 1976, "Polarized Light Scattered from Monodisperse Randomly Oriented Nonspherical Particles: Measurements," Appl. Opt., 15:384-393.
47. Zerull, R. H., 1976, "Scattering Measurements of Dielectric and Absorbing Nonspherical Particles," Beitr. Phys. Atmos., 49:168-188.
48. Greenberg, J. M., 1972, "Absorption and Emission of Radiation by Nonspherical Particles," J. Coll. Inter. Sci., 30:513-519.

DISTRIBUTION LIST

Dr. Frank D. Eaton  
Geophysical Institute  
University of Alaska  
Fairbanks, AK 99701

Commander  
US Army Aviation Center  
ATTN: ATZQ-D-MA  
Fort Rucker, AL 36362

Chief, Atmospheric Sciences Div  
Code ES-81  
NASA  
Marshall Space Flight Center,  
AL 35812

Commander  
US Army Missile R&D Command  
ATTN: DRDMI-CGA (B. W. Fowler)  
Redstone Arsenal, AL 35809

Redstone Scientific Information Center  
ATTN: DRDMI-TBD  
US Army Missile R&D Command  
Redstone Arsenal, AL 35809

Commander  
US Army Missile R&D Command  
ATTN: DRDMI-TEM (R. Haraway)  
Redstone Arsenal, AL 35809

Commander  
US Army Missile R&D Command  
ATTN: DRDMI-TRA (Dr. Essenwanger)  
Redstone Arsenal, AL 35809

Commander  
HQ, Fort Huachuca  
ATTN: Tech Ref Div  
Fort Huachuca, AZ 85613

Commander  
US Army Intelligence Center & School  
ATTN: ATSI-CD-MD  
Fort Huachuca, AZ 85613

Commander  
US Army Yuma Proving Ground  
ATTN: Technical Library  
Bldg 2100  
Yuma, AZ 85364

Naval Weapons Center (Code 3173)  
ATTN: Dr. A. Shlanta  
China Lake, CA 93555

Sylvania Elec Sys Western Div  
ATTN: Technical Reports Library  
PO Box 205  
Mountain View, CA 94040

Geophysics Officer  
PMTC Code 3250  
Pacific Missile Test Center  
Point Mugu, CA 93042

Commander  
Naval Ocean Systems Center (Code 4473)  
ATTN: Technical Library  
San Diego, CA 92152

Meteorologist in Charge  
Kwajalein Missile Range  
PO Box 67  
APO San Francisco, 96555

Director  
NOAA/ERL/APCL R31  
RB3-Room 567  
Boulder, CO 80302

Library-R-51-Tech Reports  
NOAA/ERL  
320 S. Broadway  
Boulder, CO 80302

National Center for Atmos Research  
NCAR Library  
PO Box 3000  
Boulder, CO 80307

B. Girardo  
Bureau of Reclamation  
E&R Center, Code 1220  
Denver Federal Center, Bldg 67  
Denver, CO 80225

National Weather Service  
National Meteorological Center  
W321, WWB, Room 201  
ATTN: Mr. Quiroz  
Washington, DC 20233

Director  
US Army Armament R&D Command  
Chemical Systems Laboratory  
ATTN: DRDAR-CLJ-I  
Aberdeen Proving Ground, MD 21010

Chief CB Detection & Alarms Div  
Chemical Systems Laboratory  
ATTN: DRDAR-CLC-CR (H. Tannenbaum)  
Aberdeen Proving Ground, MD 21010

Commander  
Harry Diamond Laboratories  
ATTN: DELHD-CO  
2800 Powder Mill Road  
Adelphi, MD 20783

Commander  
ERADCOM  
ATTN: DRDEL-AP  
2800 Powder Mill Road  
Adelphi, MD 20783  
2

Commander  
ERADCOM  
ATTN: DRDEL-CG/DRDEL-DC/DRDEL-CS  
2800 Powder Mill Road  
Adelphi, MD 20783

Commander  
ERADCOM  
ATTN: DRDEL-CT  
2800 Powder Mill Road  
Adelphi, MD 20783

Commander  
ERADCOM  
ATTN: DRDEL-EA  
2800 Powder Mill Road  
Adelphi, MD 20783

Commander  
ERADCOM  
ATTN: DRDEL-PA/DRDEL-ILS/DRDEL-E  
2800 Powder Mill Road  
Adelphi, MD 20783

Commander  
ERADCOM  
ATTN: DRDEL-PAO (S. Kimmel)  
2800 Powder Mill Road  
Adelphi, MD 20783

Chief  
Intelligence Materiel Dev & Support Ofc  
ATTN: DELEW-WL-I  
Bldg 4554  
Fort George G. Meade, MD 20755

Acquisitions Section, IRDB-D823  
Library & Info Service Div, NOAA  
6009 Executive Blvd  
Rockville, MD 20852

Naval Surface Weapons Center  
White Oak Library  
Silver Spring, MD 20910

The Environmental Research  
Institute of MI  
ATTN: IRIA Library  
PO Box 8618  
Ann Arbor, MI 48107

Mr. William A. Main  
USDA Forest Service  
1407 S. Harrison Road  
East Lansing, MI 48823

Dr. A. D. Belmont  
Research Division  
PO Box 1249  
Control Data Corp  
Minneapolis, MN 55440

Director  
Naval Oceanography & Meteorology  
NSTL Station  
Bay St Louis, MS 39529

Director  
US Army Engr Waterways Experiment Sta  
ATTN: Library  
PO Box 631  
Vicksburg, MS 39180

Mil Assistant for Atmos Sciences  
Ofc of the Undersecretary of Defense  
for Rsch & Engr/E&LS - Room 3D129  
The Pentagon  
Washington, DC 20301

Defense Communications Agency  
Technical Library Center  
Code 205  
Washington, DC 20305

Director  
Defense Nuclear Agency  
ATTN: Technical Library  
Washington, DC 20305

HQDA (DAEN-RDM/Dr. de Percin)  
Washington, DC 20314

Director  
Naval Research Laboratory  
Code 5530  
Washington, DC 20375

Commanding Officer  
Naval Research Laboratory  
Code 2627  
Washington, DC 20375

Dr. J. M. MacCallum  
Naval Research Laboratory  
Code 1409  
Washington, DC 20375

The Library of Congress  
ATTN: Exchange & Gift Div  
Washington, DC 20540  
2

Head, Atmos Rsch Section  
Div Atmospheric Science  
National Science Foundation  
1800 G. Street, NW  
Washington, DC 20550

CPT Hugh Albers, Exec Sec  
Interdept Committee on Atmos Science  
National Science Foundation  
Washington, DC 20550

Director, Systems R&D Service  
Federal Aviation Administration  
ATTN: ARD-54  
2100 Second Street, SW  
Washington, DC 20590

ADTC/DLODL  
Eglin AFB, FL 32542

Naval Training Equipment Center  
ATTN: Technical Library  
Orlando, FL 32813

Det 11, 2WS/OI  
ATTN: Maj Orondorff  
Patrick AFB, FL 32925

USAFETAC/CB  
Scott AFB, IL 62225

HQ, ESD/TOSI/S-22  
Hanscom AFB, MA 01731

Air Force Geophysics Laboratory  
ATTN: LCB (A. S. Carten, Jr.)  
Hanscom AFB, MA 01731

Air Force Geophysics Laboratory  
ATTN: LYD  
Hanscom AFB, MA 01731

Meteorology Division  
AFGL/LY  
Hanscom AFB, MA 01731

US Army Liaison Office  
MIT-Lincoln Lab, Library A-082  
PO Box 73  
Lexington, MA 02173

Director  
US Army Ballistic Rsch Lab  
ATTN: DRDAR-BLB (Dr. G. E. Keller)  
Aberdeen Proving Ground, MD 21005

Commander  
US Army Ballistic Rsch Lab  
ATTN: DRDAR-BLP  
Aberdeen Proving Ground, MD 21005

Commander  
US Army Tropic Test Center  
ATTN: STETC-TD (Info Center)  
APO New York 09827

Commandant  
US Army Field Artillery School  
ATTN: ATSF-CD-R (Mr. Farmer)  
Fort Sill, OK 73503

Commandant  
US Army Field Artillery School  
ATTN: ATSF-CF-R  
Fort Sill, OK 73503

Director CFD  
US Army Field Artillery School  
ATTN: Met Division  
Fort Sill, OK 73503

Commandant  
US Army Field Artillery School  
ATTN: Morris Swett Library  
Fort Sill, OK 73503

Commander  
US Army Dugway Proving Ground  
ATTN: MT-DA-L  
Dugway, UT 84022

William Peterson  
Research Associates  
Utah State University, UNC 48  
Logan, UT 84322

Inge Dirmhirn, Professor  
Utah State University, UNC 48  
Logan, UT 84322

Defense Documentation Center  
ATTN: DDC-TCA  
Cameron Station, Bldg 5  
Alexandria, VA 22314  
12

Commanding Officer  
US Army Foreign Sci & Tech Center  
ATTN: DRXST-IS1  
220 7th Street, NE  
Charlottesville, VA 22901

Naval Surface Weapons Center  
Code G65  
Dahlgren, VA 22448

Commander  
US Army Night Vision  
& Electro-Optics Lab  
ATTN: DELNV-D  
Fort Belvoir, VA 22060

Commander and Director  
US Army Engineer Topographic Lab  
ETL-TD-MB  
Fort Belvoir, VA 22060

Director  
Applied Technology Lab  
DAVDL-EU-TSD  
ATTN: Technical Library  
Fort Eustis, VA 23604

Department of the Air Force  
OL-C, 5WW  
Fort Monroe, VA 23651

Department of the Air Force  
5WW/DN  
Langley AFB, VA 23665

Director  
Development Center MCDEC  
ATTN: Firepower Division  
Quantico, VA 22134

US Army Nuclear & Chemical Agency  
ATTN: MONA-WE  
Springfield, VA 22150

Director  
US Army Signals Warfare Laboratory  
ATTN: DELSW-OS (Dr. R. Burkhardt)  
Vint Hill Farms Station  
Warrenton, VA 22186

Commander  
US Army Cold Regions Test Center  
ATTN: STECR-OP-PM  
APO Seattle, 98733

Environmental Protection Agency  
Meteorology Laboratory  
Research Triangle Park, NC 27711

US Army Research Office  
ATTN: DRXRO-PP  
PO Box 12211  
Research Triangle Park, NC 27709

Commanding Officer  
US Army Armament R&D Command  
ATTN: DRDAR-TSS Bldg 59  
Dover, NJ 07801

Commander  
HQ, US Army Avionics R&D Activity  
ATTN: DAVAA-0  
Fort Monmouth, NJ 07703

Commander/Director  
US Army Combat Surveillance & Target  
Acquisition Laboratory  
ATTN: DELCS-D  
Fort Monmouth, NJ 07703

Commander  
US Army Electronics R&D Command  
ATTN: DELCS-S  
Fort Monmouth, NJ 07703

US Army Materiel Systems  
Analysis Activity  
ATTN: DRXSY-MP  
Aberdeen Proving Ground, MD 21005

Director  
US Army Electronics Technology &  
Devices Laboratory  
ATTN: DELET-D  
Fort Monmouth, NJ 07703

Commander  
US Army Electronic Warfare Laboratory  
ATTN: DELEW-D  
Fort Monmouth, NJ 07703

Commander  
US Army Night Vision &  
Electro-Optics Laboratory  
ATTN: DELNV-L (Dr. Rudolf Buser)  
Fort Monmouth, NJ 07703

Commander  
ERADCOM Technical Support Activity  
ATTN: DELSD-L  
Fort Monmouth, NJ 07703

Project Manager, FIREFINDER  
ATTN: DRCPM-FF  
Fort Monmouth, NJ 07703

Project Manager, REMBASS  
ATTN: DRCPM-RBS  
Fort Monmouth, NJ 07703

Commander  
US Army Satellite Comm Agency  
ATTN: DRCPM-SC-3  
Fort Monmouth, NJ 07703

Commander  
ERADCOM Scientific Advisor  
ATTN: DRDEL-SA  
Fort Monmouth, NJ 07703

6585 TG/WE  
Holloman AFB, NM 88330

AFWL/WE  
Kirtland, AFB, NM 87117

AFWL/Technical Library (SUL)  
Kirtland AFB, NM 87117

Commander  
US Army Test & Evaluation Command  
ATTN: STEWS-AD-L  
White Sands Missile Range, NM 88002

Rome Air Development Center  
ATTN: Documents Library  
TSLD (Bette Smith)  
Griffiss AFB, NY 13441

Commander  
US Army Dugway Proving Ground  
ATTN: STEDP-MT-DA-M (Mr. Paul Carlson)  
Dugway, UT 84022

Commander  
TRASANA  
ATTN: DELAS-ATAA-PL  
(Dolores Anguiano)  
White Sands Missile Range, NM 88002

## ATMOSPHERIC SCIENCES RESEARCH PAPERS

1. Lindberg, J.D., "An Improvement to a Method for Measuring the Absorption Coefficient of Atmospheric Dust and other Strongly Absorbing Powders," ECOM-5565, July 1975.
2. Avara, Elton P., "Mesoscale Wind Shears Derived from Thermal Winds," ECOM-5566, July 1975.
3. Gomez, Richard B., and Joseph H. Pierluissi, "Incomplete Gamma Function Approximation for King's Strong-Line Transmittance Model," ECOM-5567, July 1975.
4. Blanco, A.J., and B.F. Engebos, "Ballistic Wind Weighting Functions for Tank Projectiles," ECOM-5568, August 1975.
5. Taylor, Fredrick J., Jack Smith, and Thomas H. Pries, "Crosswind Measurements through Pattern Recognition Techniques," ECOM-5569, July 1975.
6. Walters, D.L., "Crosswind Weighting Functions for Direct-Fire Projectiles," ECOM-5570, August 1975.
7. Duncan, Louis D., "An Improved Algorithm for the Iterated Minimal Information Solution for Remote Sounding of Temperature," ECOM-5571, August 1975.
8. Robbiani, Raymond L., "Tactical Field Demonstration of Mobile Weather Radar Set AN/TPS-41 at Fort Rucker, Alabama," ECOM-5572, August 1975.
9. Miers, B., G. Blackman, D. Langer, and N. Lorimier, "Analysis of SMS/GOES Film Data," ECOM-5573, September 1975.
10. Manquero, Carlos, Louis Duncan, and Rufus Bruce, "An Indication from Satellite Measurements of Atmospheric CO<sub>2</sub> Variability," ECOM-5574, September 1975.
11. Petracca, Carmine, and James D. Lindberg, "Installation and Operation of an Atmospheric Particulate Collector," ECOM-5575, September 1975.
12. Avara, Elton P., and George Alexander, "Empirical Investigation of Three Iterative Methods for Inverting the Radiative Transfer Equation," ECOM-5576, October 1975.
13. Alexander, George D., "A Digital Data Acquisition Interface for the SMS Direct Readout Ground Station — Concept and Preliminary Design," ECOM-5577, October 1975.
14. Cantor, Israel, "Enhancement of Point Source Thermal Radiation Under Clouds in a Nonattenuating Medium," ECOM-5578, October 1975.
15. Norton, Colburn, and Glenn Hoidale, "The Diurnal Variation of Mixing Height by Month over White Sands Missile Range, N.M.," ECOM-5579, November 1975.
16. Avara, Elton P., "On the Spectrum Analysis of Binary Data," ECOM-5580, November 1975.
17. Taylor, Fredrick J., Thomas H. Pries, and Chao-Huan Huang, "Optimal Wind Velocity Estimation," ECOM-5581, December 1975.
18. Avara, Elton P., "Some Effects of Autocorrelated and Cross-Correlated Noise on the Analysis of Variance," ECOM-5582, December 1975.
19. Gillespie, Patti S., R.L. Armstrong, and Kenneth O. White, "The Spectral Characteristics and Atmospheric CO<sub>2</sub> Absorption of the Ho<sup>+</sup>3:YLF Laser at 2.05 $\mu$ m," ECOM-5583, December 1975.
20. Novlan, David J. "An Empirical Method of Forecasting Thunderstorms for the White Sands Missile Range," ECOM-5584, February 1976.
21. Avara, Elton P., "Randomization Effects in Hypothesis Testing with Autocorrelated Noise," ECOM-5585, February 1976.
22. Watkins, Wendell R., "Improvements in Long Path Absorption Cell Measurement," ECOM-5586, March 1976.
23. Thomas, Joe, George D. Alexander, and Marvin Dubbin, "SATTEL — An Army Dedicated Meteorological Telemetry System," ECOM-5587, March 1976.
24. Kennedy, Bruce W., and Delbert Bynum, "Army User Test Program for the RDT&E-XM-75 Meteorological Rocket," ECOM-5588, April 1976.

25. Barnett, Kenneth M., "A Description of the Artillery Meteorological Comparisons at White Sands Missile Range, October 1974 - December 1974 ('PASS' - Prototype Artillery [Meteorological] Subsystem)," ECOM-5589, April 1976.
26. Miller, Walter B., "Preliminary Analysis of Fall-of-Shot From Project 'PASS'," ECOM-5590, April 1976.
27. Avara, Elton P., "Error Analysis of Minimum Information and Smith's Direct Methods for Inverting the Radiative Transfer Equation," ECOM-5591, April 1976.
28. Yee, Young P., James D. Horn, and George Alexander, "Synoptic Thermal Wind Calculations from Radiosonde Observations Over the Southwestern United States," ECOM-5592, May 1976.
29. Duncan, Louis D., and Mary Ann Seagraves, "Applications of Empirical Corrections to NOAA-4 VTPR Observations," ECOM-5593, May 1976.
30. Miers, Bruce T., and Steve Weaver, "Applications of Meteorological Satellite Data to Weather Sensitive Army Operations," ECOM-5594, May 1976.
31. Sharenow, Moses, "Redesign and Improvement of Balloon ML-566," ECOM-5595, June, 1976.
32. Hansen, Frank V., "The Depth of the Surface Boundary Layer," ECOM-5596, June 1976.
33. Pinnick, R.G., and E.B. Stenmark, "Response Calculations for a Commercial Light-Scattering Aerosol Counter," ECOM-5597, July 1976.
34. Mason, J., and G.B. Hoidale, "Visibility as an Estimator of Infrared Transmittance," ECOM-5598, July 1976.
35. Bruce, Rufus E., Louis D. Duncan, and Joseph H. Pierluissi, "Experimental Study of the Relationship Between Radiosonde Temperatures and Radiometric-Area Temperatures," ECOM-5599, August 1976.
36. Duncan, Louis D., "Stratospheric Wind Shear Computed from Satellite Thermal Sounder Measurements," ECOM-5800, September 1976.
37. Taylor, F., P. Mohan, P. Joseph and T. Pries, "An All Digital Automated Wind Measurement System," ECOM-5801, September 1976.
38. Bruce, Charles, "Development of Spectrophones for CW and Pulsed Radiation Sources," ECOM-5802, September 1976.
39. Duncan, Louis D., and Mary Ann Seagraves, "Another Method for Estimating Clear Column Radiances," ECOM-5803, October 1976.
40. Blanco, Abel J., and Larry E. Taylor, "Artillery Meteorological Analysis of Project Pass," ECOM-5804, October 1976.
41. Miller, Walter, and Bernard Engebos, "A Mathematical Structure for Refinement of Sound Ranging Estimates," ECOM-5805, November, 1976.
42. Gillespie, James B., and James D. Lindberg, "A Method to Obtain Diffuse Reflectance Measurements from 1.0 to 3.0  $\mu\text{m}$  Using a Cary 17I Spectrophotometer," ECOM-5806, November 1976.
43. Rubio, Roberto, and Robert O. Olsen, "A Study of the Effects of Temperature Variations on Radio Wave Absorption," ECOM-5807, November 1976.
44. Ballard, Harold N., "Temperature Measurements in the Stratosphere from Balloon-Borne Instrument Platforms, 1968-1975," ECOM-5808, December 1976.
45. Monahan, H.H., "An Approach to the Short-Range Prediction of Early Morning Radiation Fog," ECOM-5809, January 1977.
46. Engebos, Bernard Francis, "Introduction to Multiple State Multiple Action Decision Theory and Its Relation to Mixing Structures," ECOM-5810, January 1977.
47. Low, Richard D.H., "Effects of Cloud Particles on Remote Sensing from Space in the 10-Micrometer Infrared Region," ECOM-5811, January 1977.
48. Bonner, Robert S., and R. Newton, "Application of the AN/GVS-5 Laser Rangefinder to Cloud Base Height Measurements," ECOM-5812, February 1977.
49. Rubio, Roberto, "Lidar Detection of Subvisible Reentry Vehicle Erosive Atmospheric Material," ECOM-5813, March 1977.
50. Low, Richard D.H., and J.D. Horn, "Mesoscale Determination of Cloud-Top Height: Problems and Solutions," ECOM-5814, March 1977.

51. Duncan, Louis D., and Mary Ann Seagraves, "Evaluation of the NOAA-4 VTPR Thermal Winds for Nuclear Fallout Predictions," ECOM-5815, March 1977.
52. Randhawa, Jagir S., M. Izquierdo, Carlos McDonald and Zvi Salpeter, "Stratospheric Ozone Density as Measured by a Chemiluminescent Sensor During the Stratcom VI-A Flight," ECOM-5816, April 1977.
53. Rubio, Roberto, and Mike Izquierdo, "Measurements of Net Atmospheric Irradiance in the 0.7- to 2.8-Micrometer Infrared Region," ECOM-5817, May 1977.
54. Ballard, Harold N., Jose M. Serna, and Frank P. Hudson Consultant for Chemical Kinetics, "Calculation of Selected Atmospheric Composition Parameters for the Mid-Latitude, September Stratosphere," ECOM-5818, May 1977.
55. Mitchell, J.D., R.S. Sagar, and R.O. Olsen, "Positive Ions in the Middle Atmosphere During Sunrise Conditions," ECOM-5819, May 1977.
56. White, Kenneth O., Wendell R. Watkins, Stuart A. Schleusener, and Ronald L. Johnson, "Solid-State Laser Wavelength Identification Using a Reference Absorber," ECOM-5820, June 1977.
57. Watkins, Wendell R., and Richard G. Dixon, "Automation of Long-Path Absorption Cell Measurements," ECOM-5821, June 1977.
58. Taylor, S.E., J.M. Davis, and J.B. Mason, "Analysis of Observed Soil Skin Moisture Effects on Reflectance," ECOM-5822, June 1977.
59. Duncan, Louis D. and Mary Ann Seagraves, "Fallout Predictions Computed from Satellite Derived Winds," ECOM-5823, June 1977.
60. Snider, D.E., D.G. Murcray, F.H. Murcray, and W.J. Williams, "Investigation of High-Altitude Enhanced Infrared Background Emissions" (U), SECRET, ECOM-5824, June 1977.
61. Dubbin, Marvin H. and Dennis Hall, "Synchronous Meteorological Satellite Direct Readout Ground System Digital Video Electronics," ECOM-5825, June 1977.
62. Miller, W., and B. Engebos, "A Preliminary Analysis of Two Sound Ranging Algorithms," ECOM-5826, July 1977.
63. Kennedy, Bruce W., and James K. Luers, "Ballistic Sphere Techniques for Measuring Atmospheric Parameters," ECOM-5827, July 1977.
64. Duncan, Louis D., "Zenith Angle Variation of Satellite Thermal Sounder Measurements," ECOM-5828, August 1977.
65. Hansen, Frank V., "The Critical Richardson Number," ECOM-5829, September 1977.
66. Ballard, Harold N., and Frank P. Hudson (Compilers), "Stratospheric Composition Balloon-Borne Experiment," ECOM-5830, October 1977.
67. Barr, William C., and Arnold C. Peterson, "Wind Measuring Accuracy Test of Meteorological Systems," ECOM-5831, November 1977.
68. Ethridge, G.A. and F.V. Hansen, "Atmospheric Diffusion: Similarity Theory and Empirical Derivations for Use in Boundary Layer Diffusion Problems," ECOM-5832, November 1977.
69. Low, Richard D.H., "The Internal Cloud Radiation Field and a Technique for Determining Cloud Blackness," ECOM-5833, December 1977.
70. Watkins, Wendell R., Kenneth O. White, Charles W. Bruce, Donald L. Walters, and James D. Lindberg, "Measurements Required for Prediction of High Energy Laser Transmission," ECOM-5834, December 1977.
71. Rubio, Robert, "Investigation of Abrupt Decreases in Atmospherically Backscattered Laser Energy," ECOM-5835, December 1977.
72. Monahan, H.H. and R.M. Cionco, "An Interpretative Review of Existing Capabilities for Measuring and Forecasting Selected Weather Variables (Emphasizing Remote Means)," ASL-TR-0001, January 1978.
73. Heaps, Melvin G., "The 1979 Solar Eclipse and Validation of D-Region Models," ASL-TR-0002, March 1978.

74. Jennings, S.G., and J.B. Gillespie, "M.I.E. Theory Sensitivity Studies - The Effects of Aerosol Complex Refractive Index and Size Distribution Variations on Extinction and Absorption Coefficients Part II: Analysis of the Computational Results," ASL-TR-0003, March 1978.
75. White, Kenneth O. et al, "Water Vapor Continuum Absorption in the 3.5 $\mu$ m to 4.0 $\mu$ m Region," ASL-TR-0004, March 1978.
76. Olsen, Robert O., and Bruce W. Kennedy, "ABRES Pretest Atmospheric Measurements," ASL-TR-0005, April 1978.
77. Ballard, Harold N., Jose M. Serna, and Frank P. Hudson, "Calculation of Atmospheric Composition in the High Latitude September Stratosphere," ASL-TR-0006, May 1978.
78. Watkins, Wendell R. et al, "Water Vapor Absorption Coefficients at HF Laser Wavelengths," ASL-TR-0007, May 1978.
79. Hansen, Frank V., "The Growth and Prediction of Nocturnal Inversions," ASL-TR-0008, May 1978.
80. Samuel, Christine, Charles Bruce, and Ralph Brewer, "Spectrophone Analysis of Gas Samples Obtained at Field Site," ASL-TR-0009, June 1978.
81. Pinnick, R.G. et al., "Vertical Structure in Atmospheric Fog and Haze and its Effects on IR Extinction," ASL-TR-0010, July 1978.
82. Low, Richard D.H., Louis D. Duncan, and Richard B. Gomez, "The Microphysical Basis of Fog Optical Characterization," ASL-TR-0011, August 1978.
83. Heaps, Melvin G., "The Effect of a Solar Proton Event on the Minor Neutral Constituents of the Summer Polar Mesosphere," ASL-TR-0012, August 1978.
84. Mason, James B., "Light Attenuation in Falling Snow," ASL-TR-0013, August 1978.
85. Blanco, Abel J., "Long-Range Artillery Sound Ranging: "PASS" Meteorological Application," ASL-TR-0014, September 1978.
86. Heaps, M.G., and F.E. Niles, "Modeling the Ion Chemistry of the D-Region: A case Study Based Upon the 1966 Total Solar Eclipse," ASL-TR-0015, September 1978.
87. Jennings, S.G., and R.G. Pinnick, "Effects of Particulate Complex Refractive Index and Particle Size Distribution Variations on Atmospheric Extinction and Absorption for Visible Through Middle-Infrared Wavelengths," ASL-TR-0016, September 1978.

DEPARTMENT OF THE ARMY  
US ARMY ATMOSPHERIC SCIENCES LABORATORY  
DELAS-DM-A  
WHITE SANDS MISSILE RANGE, NM 88002

OFFICIAL BUSINESS

Penalty For Private Use, \$300

POSTAGE AND FEES PAID  
DEPARTMENT OF THE ARMY  
DOD 314

